be the major aetiologic agent inducing neuronal cell dysfunction or death and other debilitating neurological and behaviour consequences of HIV-1 infection observed in HAD and HE. Gp120 causes neuronal damage by stimulating MP to release neurotoxins such as cytokines and chemokines. It may also act on neuronal cells directly by binding to neuronal CXCR4 receptors (Horuk *et al.*, 1997; Kaul *et al.*, 2001), producing an increase in intracellular free calcium concentration $[Ca^{2+}]_i$ (Dreyer *et al.*, 1990; Medina *et al.*, 1999). Interestingly, gp120 was found to induce two different types of $[Ca^{2+}]_i$ oscillation in primary hippocampal neuronal cultures. One type of $[Ca^{2+}]_i$ oscillation required the maintained presence of gp120 and ceased when gp120 was removed from the bath, and the other type of oscillations persisted long after washout of gp120 (Lo *et al.*, 1992). The gp120-induced $[Ca^{2+}]_i$ oscillations were completely blocked by antagonists of Na^+ and NMDA-gated ion channels, suggesting that they might be mediated via network-driven synaptic events (Lo *et al.*, 1992).

In immature brains, spontaneously occurring neuronal oscillations constitute a hallmark of developmental networks and participate in activity-dependent brain growth and synapse formation (Ben-Ari, 2001). These neuronal oscillations, so-called 'giant depolarizing potentials' (GDPs), result in calcium influx through NMDA receptor channels and voltage-gated calcium channels (Khazipov *et al.*, 1997). However, uncontrolled and excessive accumulation of $[Ca^{2+}]_i$ is considered as the unifying theme in a number of cytotoxic processes that lead to neuronal dysfunction and apoptosis (Hesselgesser *et al.*, 1998). To understand how HIV-1 alters neuronal function in the developing nervous system, we studied the effects of HIV-1 gp120 on GDPs recorded in the CA3 pyramidal cells in neonatal rat hippocampal slices. We found that gp120 enhanced GDP frequency through CXCR4, a chemokine receptor expressed in both glial cells (astrocyte and microglia) and specific subsets of neurons (Asensio & Campbell, 1999). An abstract form of these results was presented at the 2004 Society for Neuroscience 34th Annual Meeting in San Diego, CA, USA.

Materials and methods

Materials

HIV-1 $gp120_{MN}$ was obtained from the National Institute of Health (NIH) AIDS Research and Reference Reagent Program (Rockville, MD, USA). Aliquots of gp120 were kept as 200 ng/μL stock solution at −80 °C. The stock solution was diluted to the desired concentrations with artificial cerebrospinal fluid (ACSF) 2–5 min before application. Stromal cell-derived factor-1α (SDF-1α) was purchased from R & D Systems (Minneapolis, MN, USA). Fura-2 AM was obtained from Molecular Probes (Eugene, OR, USA). Neurobasal media was purchased from Invitrogen Corp (Carlsbad, CA, USA). T140 was obtained from Kyoto University (Sakyo-ku, Kyoto, Japan). All chemicals, unless otherwise specified, were from Sigma (St. Louis, MO, USA).

Primary hippocampal-cortical neuronal cultures

Pregnant Sprague-Dawley rats were anaesthetized with isoflurane and embryonic rats (17–18-day-old) were dissected out under sterile conditions. The fetal rats were decapitated and hippocampal and cortical tissues collected. Individual cells were mechanically dissociated by trituration in a Ca^{2+}/Mg^{2+}-free Hank's balanced salt solution (HBSS) after 30 min of trypsin (0.1%) digestion at 37 °C. Trypsin was neutralized with 10% fetal bovine serum (FBS, 10%) and the cell suspension washed three times in HBSS and resuspended in neurobasal medium (Invitrogen Corp, Carlsbad, CA, USA) supplemented with 2 mM glutamine, 50 μg/mL penicillin and streptomycin and B27. Cells were seeded in poly D-lysine coated cover slips at a concentration of 250 000 cells/mL. The cells were used for Ca^{2+} imaging after 12–14 days in culture.

Calcium flux analysis

Cells were loaded with 5 μM Fura-2 AM using the procedure as previously described. Fura-2 fluorescence was imaged with an inverted Nikon TMD Diaphot epifluorescent microscope (40× water immersion lens). The change in free Ca^{2+} was measured by monitoring the intensity of excitation emission at 510 nm in response to repeated sequential excitation at 340 nm and 380 nm using a digital camera (Photometrics, Huntington Beach, CA). Excitation control, image acquisition and off-line analysis of images were performed using Axon Imaging Workbench-2 (Axon Instruments). The selection of neuronal cells for Ca^{2+} imaging was based on cell morphology and the selected cells in the image were analysed independently for each time point in the captured sequence. Data are presented as the relative ratio of fluorescence at 340 nm and 380 nm.

Hippocampal brain slice preparation

Hippocampal brain slices were prepared from postnatal day 2 (P2) to P6 Sprague–Dawley rats of either sex as described previously (Kasyanov *et al.*, 2004). Briefly, rats were anaesthetized with isoflurane and decapitated. The brain was quickly removed from the skull and submerged in ACSF containing (in mM): NaCl 126, KCl 3.5, $CaCl_2$ 2, $MgCl_2$ 1.3, NaH_2PO_4 1.2, $NaHCO_3$ 25, glucose 11, and saturated with 95% O_2 and 5% CO_2 (pH 7.3–7.4). Coronal hippocampal slices (500 μm in thickness) were cut with a vibrating microslicer (World Precision Instruments, Sarasota, FL, USA) and incubated at room temperature in oxygenated ACSF for at least 1 h before use. Individual slices were transferred to the recording chamber and superfused with ACSF at 2.5–3.0 mL/min at 34 °C. The Institutional Animal Care and Use Committee (IACUC) of University of Nebraska Medical Center strictly reviewed all animal use procedures (IACUC # 00-062-07).

Electrophysiology and data analyses

Whole-cell current-clamp recordings were performed on CA3 pyramidal cells in hippocampal slices using a 'blind' method. Spontaneous GDPs and excitatory postsynaptic potentials (EPSPs) were recorded and amplified using an Axopatch-1D amplifier (Axon Instruments, Union City, CA, USA), filtered at 1 kHz, and digitized at 5 kHz through a Digidata 1322A (Axon Instruments). To minimize potential 'contamination' of the EPSPs by spontaneous action potentials, the cells were hyperpolarized to −80 mV PCLAMP 8 software (Axon Instruments) was used for data acquisition (gap-free configuration) and the data was stored in a PC computer. The patch electrodes were made from borosilicate glass capillaries (World Precision Instruments) and had a resistance of 5–7 MΩ when filled with intracellular solution containing (in mM): KCl 140, HEPES 10, EGTA 1, $MgCl_2$ 1, MgATP 2 (pH 7.3 with KOH, osmolarity 280–290 mOsm). The whole cell capacitance was fully compensated and the series resistance (10–20 MΩ) was compensated at 75–80%. Membrane input resistance was calculated by measuring membrane voltage change in response to small hyperpolarizing current pulses (300 ms in duration) across the cell membrane. Series resistance was monitored throughout the recordings. A cell was discarded if it changed significantly (> 20% of the control). Both PCLAMP 8 and Mini Analysis Program

(Synaptosoft Inc, Decatur, GA, USA) were employed for data analyses. For each cell, the mean GDP frequency was calculated before (control), during (starting 1 min after the onset of drug perfusion) and after (washout) drug application. Statistical comparisons were made between mean values (control vs. drug treatment). The numerical data are given as mean ± SD and compared using the Student's *t*-test or Kolmogorov–Smirnov (K–S) test. The differences were considered significant when $P < 0.05$.

Results

HIV-1 gp120 increases GDP frequency in CA3 pyramidal cells

To understand how HIV-1 gp120 affects neuronal activity in developing nervous system, we studied the effects of HIV-1 gp120 on GDPs recorded from CA3 pyramidal cells in hippocampal brain slices taken from neonatal rats (P2–P6). Under whole-cell current clamp, the CA3 pyramidal cells fire spontaneous GDPs. The occurrence of GDPs was random and independent of cell membrane potential, with an average firing frequency of 0.088 ± 0.015 Hz ($n = 26$). The spontaneous GDPs were blocked either by the $GABA_A$ receptor antagonist, picrotoxin, (100 μM, $n = 5$) or by the Na^+ channel blocker, tetrodoxin (TTX, 0.1 μM, $n = 4$), but not by the NMDA receptor antagonist, 2-amino-5-phosphovalerate (APV, 50 μM, $n = 4$, data not shown). These results suggest that GDPs were GABA-mediated, network-driven events. In order to evaluate whether HIV-1 gp120 affects GDP occurrence, we exposed hippocampal brain slices to gp120 through bath perfusion. Bath application of gp120 produced a long-lasting enhancement of GDP firing frequency in CA3 pyramidal cells in a concentration-dependent manner (Fig. 1). When slices were perfused with gp120 at concentrations of 2, 20, and 200 pM, respectively, the average GDP frequency (Hz) was from 0.095 ± 0.010 to 0.089 ± 0.010 ($n = 3$), 0.123 ± 0.003 to 0.152 ± 0.006 ($n = 3$), and 0.045 ± 0.003 to 0.071 ± 0.002 Hz ($n = 6$), respectively (Fig. 1D). The enhancement occurred 3–5 min after gp120 reached the recording chamber and lasted for >15 min during the washout period (Fig. 1A–C). While it enhanced the occurrence of GDPs, gp120 had no significant ($P > 0.05$, $n = 5$) effects on spontaneous mini EPSPs. The average mini-EPSP occurring frequency was 3.6 ± 1.3 Hz in control, 3.6 ± 1.1 Hz during application of gp120, and 2.8 ± 0.7 Hz during the wash period (Fig. 2; $n = 5$). Application of gp120 did not

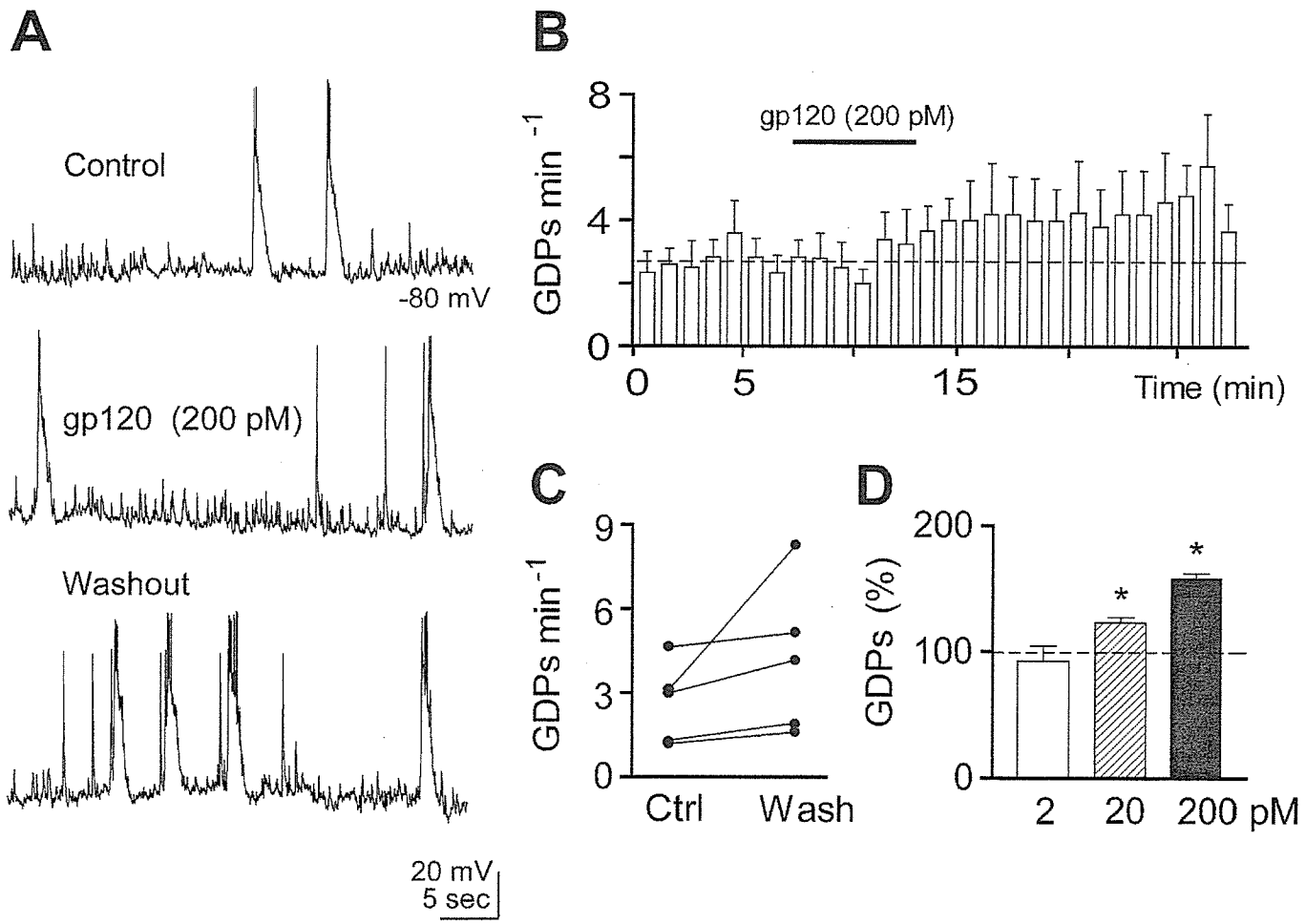

FIG. 1. HIV-1 gp120 produces persistent enhancement of GDP firing frequency. Panel A shows the representative traces recorded under current clamp from a CA3 pyramidal neuron (P4) under control (upper), during bath application of gp120 (middle), and 5 min after washout started (lower). Note the increase of GDP firing during the washout period. Panel B is the time course illustrating the average GDP frequency before, during, and after gp120 application ($n = 5$). Each bar represents the number of GDPs recorded in 1 min. The dotted line represents the mean GDP frequency under control conditions. The horizontal bar indicates bath application of gp120 (200 pM). Panel C plots GDP frequencies recorded from five individual cells (as shown in panel B) during control and 5 min after washout started. Panel D is a summarized bar graph illustrating the relationship of average GDP frequency as a function of gp120 concentrations. Each bar represents the percentage of changing of the GDP frequency induced by gp120 at 2, 20, 200 pM, respectively. *$P < 0.05$

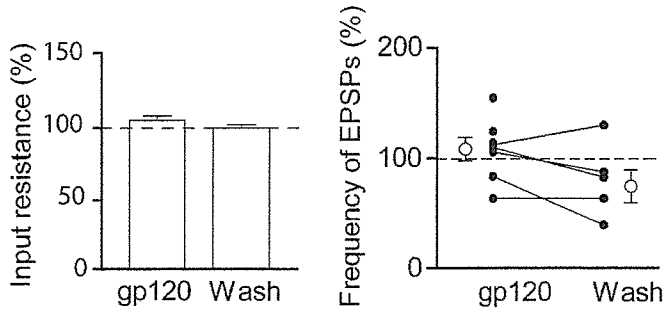

FIG. 2. HIV-1 gp120 had no significant effects on membrane input resistance (A) and spontaneous EPSPs (B). The membrane input resistance (A) was 103.2 ± 3.2% of control level (dashed line) during bath perfusion of gp120 and 97.9 ± 2.0% of control level during washout period. Panel B shows the spontaneous EPSP frequency recorded from individual neurons during bath application of gp120 ($n = 7$, filled circles) and 5 min after the start of wash ($n = 5$, filled circles), expressed as percentage of control level (dashed line). The open circles represent the average EPSP frequency during bath application of gp120 (left) and 5 min after the start of wash (right).

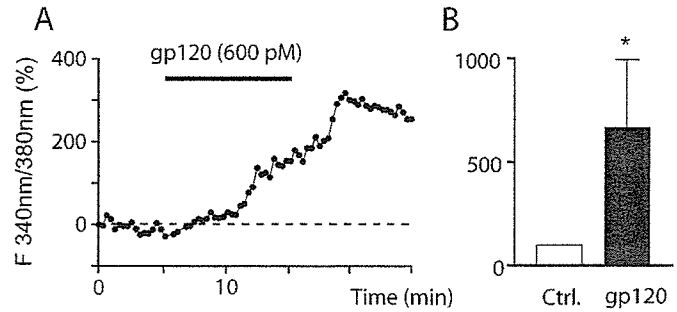

FIG. 3. gp120 evoked an increase of intracellular Ca^{2+} concentration in fetal rat hippocampal-cortical neuronal cultures. Panel A (left) shows an example of the change of fluorescence ratio in response to bath application of gp120 (600 pM). Panel B (right) illustrates the average of fluorescence ratio measured before (Ctrl) and 10 min after bath application of gp120 (gp120, $n = 4$). Note that gp120 induced a significant increase of the relative ratio of fluorescence at 340 and 380 nM, suggesting a rise of intracellular Ca^{2+} concentration induced by gp120.

produce a significant change in either cell resting membrane potential, or cell membrane input resistance. The average resting membrane potentials before, during, and after application of gp120 were 89 ± 7 mV, 95 ± 8 mV, and 92 ± 12 mV, respectively ($n = 6$). The average membrane input resistance was 103.2 ± 3.2% of the basal level ($n = 3$) during bath application of gp120 and 97.9 ± 2.0% of the basal level ($n = 3$) when measured during the wash period (Fig. 2).

Gp120 induces a persistent increase in intracellular calcium in neurons

GDPs increase the levels of $[Ca^{2+}]_i$ through activation of voltage-gated Ca^{2+} channels (Leinekugel *et al.*, 1995) and/or by reducing the voltage-dependent Mg^{2+} blockade of NMDA receptor channels and resultant activation of NMDA receptors, resulting in a further rise of $[Ca^{2+}]_i$ (Leinekugel *et al.*, 1997). We hypothesized that the enhancement of GDP frequency by gp120 may cause substantial increase of intracellular Ca^{2+} levels. To test this hypothesis, we measured $[Ca^{2+}]_i$ in primary fetal rat hippocampal-cortical neuronal cultures. Utilizing the single cell calcium imaging system at the Center for Neuroviology and Neurodegenerative Disorders, we indeed demonstrated in four out of ten cells a profound calcium response in the presence of gp120 (Fig. 3), with an average fluorescence ratio of 668 ± 326% (mean ± SD, $n = 4$). In comparison with the fluorescence ratio detected in untreated controls, the difference is statistically significant ($P < 0.05$), suggesting that gp120 increases GDP frequency and intracellular Ca^{2+} levels.

Blockade of gp120-induced enhancement of GDPs by T140, an antagonist for chemokine receptor CXCR4

Gp120 interacts with CXCR4 receptors and the receptors have been detected in human fetal neuronal and glial cell cultures (Zheng *et al.*, 1999; Croitoru-Lamoury *et al.*, 2003), and in neurons from autopsy brain tissues in children (Vallat *et al.*, 1998) and adults (Lavi *et al.*, 1997; Lavi *et al.*, 1998). To examine if the gp120-induced increase of GDP occurrence is mediated through activation of chemokine receptor CXCR4, we tested the effects of T140, a highly selective CXCR4 receptor antagonist that has recently been shown to strongly suppress HIV-1 entry into target cells by blocking viral gp120 binding to CXCR4 receptors (Tamamura & Fujii, 2004), on gp120-induced enhancement of GDP occurrence. While it had no significant effect on spontaneous GDP occurrence when applied by bath (Fig. 4A; $n = 5$), T140 (50 nM) significantly blocked gp120-induced enhancement of GDP frequency (Fig. 4A and B; $n = 5$). The blockade of gp120-induced enhancement of spontaneous GDPs by CXCR4 receptor

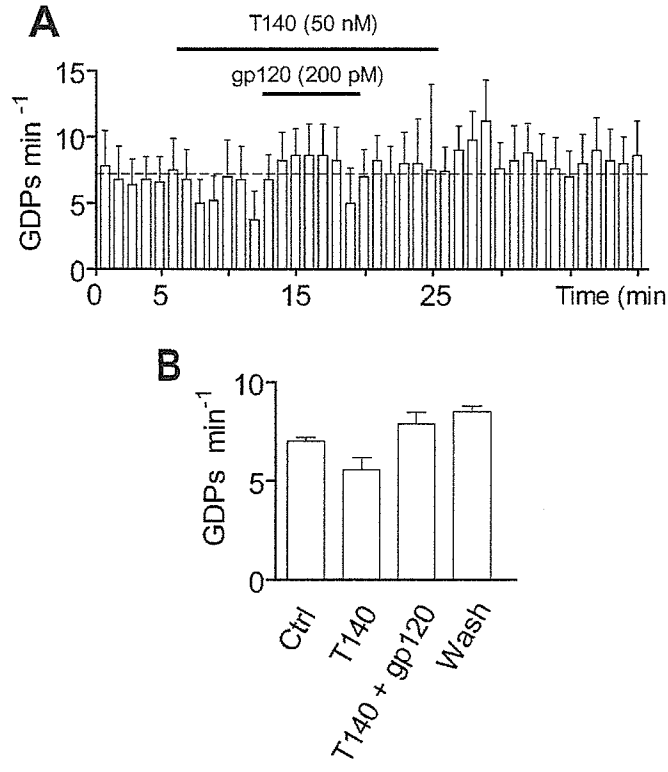

FIG. 4. Blockade of the HIV-1 gp120-induced enhancement of GDP occurrence by T140, a specific CXCR4 receptor antagonist. (A) Time course showing the averaged GDP firing frequency for five cells. Each column represents the number of GDPs recorded in 1 min. The dotted line represents the mean GDP frequency under control conditions. Note that gp120 failed to increase GDP frequency in the presence of T140. (B) Each bar represents the mean GDP frequency observed in five neurons during control, application of T140 (50 nM, before gp120 application), T140 plus gp120 (200 pM), and wash. Error bars represent the SEM.

antagonist suggests that gp120 increases GDP frequency through CXCR4 receptors.

SDF-1α mimics the effects of gp120 on the GDP

To explore further whether gp120-induced enhancement of GDP frequency occurs through CXCR4 receptors, we examined the effects of SDF-1α, the only ligand for CXCR4 receptors, on GDP frequency in CA3 pyramidal cells. Bath application of SDF-1α (50 nM) induced biphasic effects on GDP firing frequency, with an initial decrease from 0.115 ± 0.007 Hz to 0.064 ± 0.014 Hz followed by a significant increase from 0.115 ± 0.007 Hz to 0.142 ± 0.006 Hz (Fig. 5A–C; $n = 5$) during the wash period. The depressive effect of SDF-1α was rapid in onset, reaching maximum effect in 2–3 min, and the recovery was attained 3–5 min after starting the washout (Fig. 5B). SDF-1α did not alter the resting membrane potential, membrane input resistance, or the shape of GDPs. The membrane potentials before, during, and after application of SDF-1α were −80 ± 6 mV, −80 ± 5 mV, and −85 ± 1 mV, respectively. Membrane input resistance were 99.1 ± 7.2% of the basal level during application of SDF-1α and 107 ± 18.7% of the basal level during the wash period ($n = 3$). The differences were not statistically significant ($P > 0.05$). Like gp120, SDF-1α did not produce significant effects on spontaneous mini-EPSPs, with an average frequency of 1.43 ± 0.34 Hz in control and 1.61 ± 0.27 Hz during application of SDF-1α ($n = 3$, $P > 0.05$, K–S test). These results demonstrated that SDF-1α mimicked the effects of gp120 on GDPs, providing further evidence supporting our hypothesis that gp120 increases GDP frequency through CXCR4 receptors.

H7 blocked the effects of gp120 on GDPs

It has been shown that gp120 activates protein kinase C (PKC) in the hippocampus (Zorn *et al.*, 1990) and induces apoptosis in primary endothelium through PKC (Huang & Bond, 2000). We hypothesize that gp120 may increase GDP frequency through activation of PKC and/or cAMP-dependent protein kinase (PKA). To test this hypothesis, we examined the effects of H7, an inhibitor for PKA and PKC, on gp120-induced enhancement of GDP occurrence in neonatal hippocampal slices. When applied alone, H7 (100 μM) inhibited GDP occurrence ($n = 4$), showing the involvement of PKA and/or PKC in the occurrence of spontaneous GDPs. However, when coapplied with gp120, H7 blocked the gp120-associated increase of GDP frequency (Fig. 6A). The average GDP frequency before (control) and after coapplication of H7 and gp120 were 0.080 ± 0.005 Hz and 0.060 ± 0.003 Hz ($n = 4$), respectively. In comparison with the GDP frequency occurred after bath application of gp120 (Fig. 1D), the difference was statistically significant ($P < 0.05$), suggesting the involvement of PKA/PKC in gp120-induced increase of GDPs. To verify whether activation of PKA enhances GDPs, we tested the effects of the adenylyl cyclase stimulator, forskolin, on GDP frequency. Our results showed that forskolin mimicked the effects of gp120 on GDPs (Fig. 6B), illustrating that the cAMP-dependent protein kinase may also be involved in gp120-induced enhancement of GDPs. Taken together, these results suggest that gp120 increases GDP firing frequency through a CXCR4 receptor-PKA/C signal pathway.

Discussion

In this study, we demonstrated that the HIV-1 envelope glycoprotein, gp120, induced a persistent increase of network-driven, GABA-mediated GDP firing frequency in the CA3 pyramidal cells in neonatal rat hippocampal slices. HIV-1 gp120 enhances neuronal spontaneous GDP firing frequency in a concentration-dependent manner without affecting the neuronal resting membrane potential and membrane input resistance, suggesting that the site of action for gp120 is most likely on the neural network, other than on the neurons recorded. The

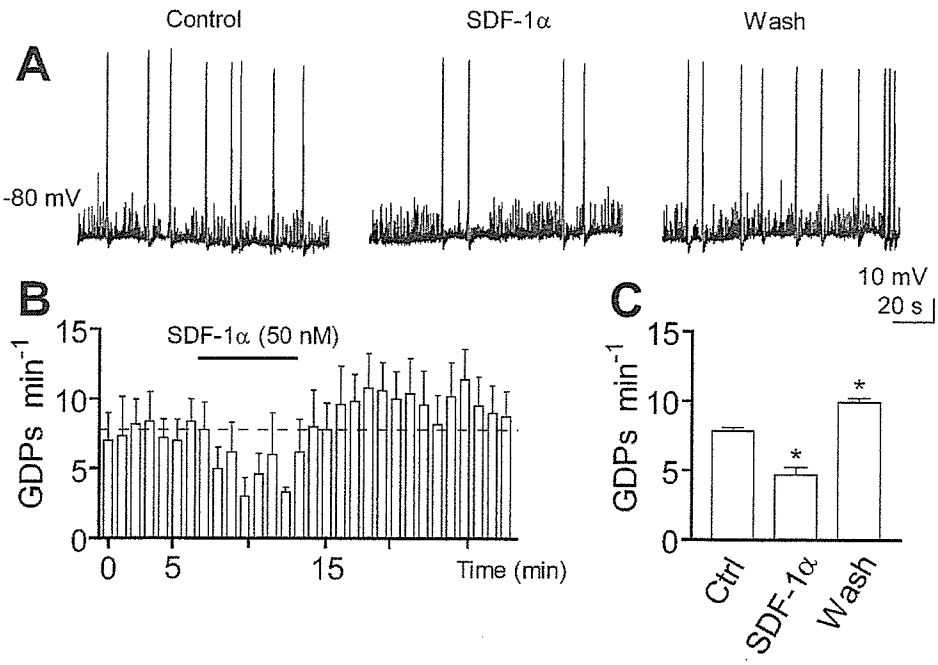

FIG. 5. SDF-1α, the only ligand for the chemokine receptor, CXCR4, modulates the GDP firing frequency. (A) Representative spontaneous GDPs recorded from a CA3 pyramidal neuron at P3 before (control), during (SDF-1α) and after (wash) bath application of SDF-1α (50 nM). (B) Time course showing the effects of SDF-1α on spontaneous GDP frequency ($n = 5$). Each column represents the number of GDPs recorded in 1 min. The dotted line represents the mean GDP frequency under control conditions. (C) The bar graph depicts the average GDP frequencies sampled before, during, and after SDF-1α application. Data represent mean ± SD from five neurons. *$P < 0.05$ when compared with Ctrl.

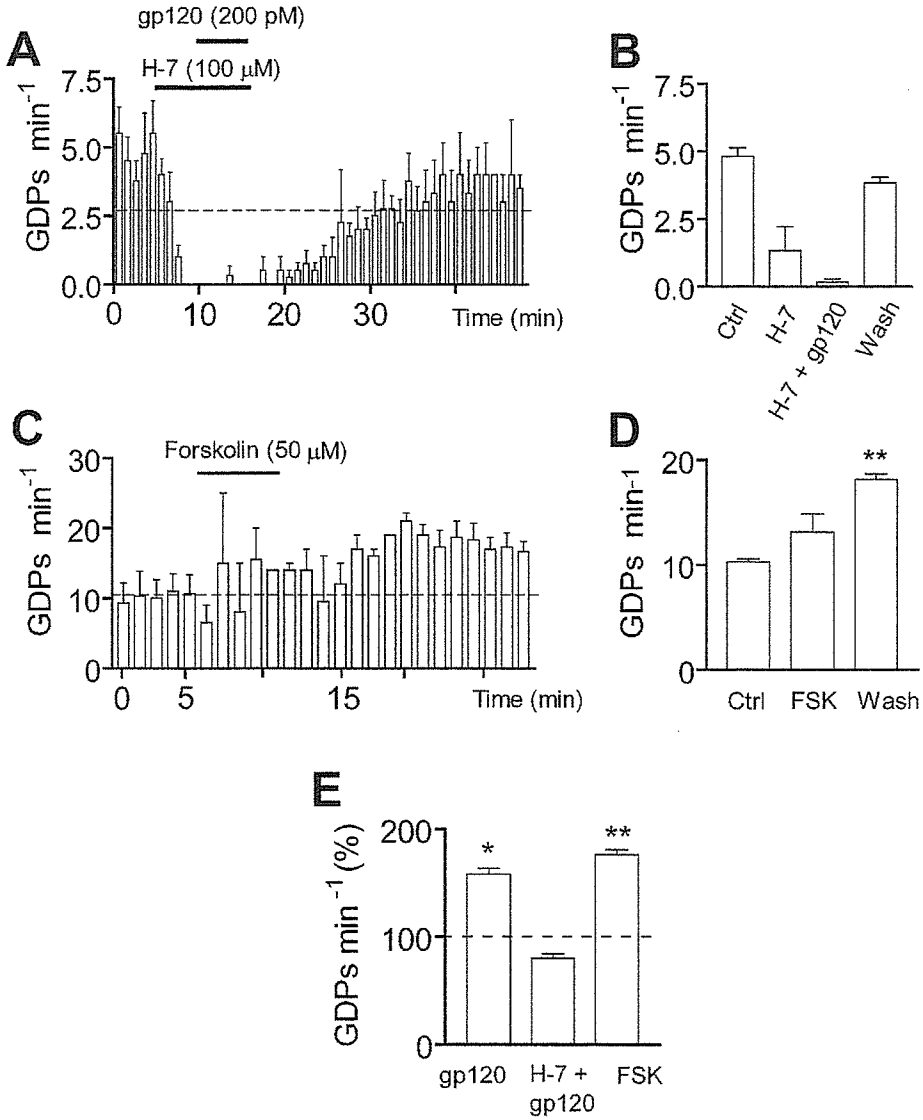

FIG. 6. Involvement of protein kinase A/C in gp120-induced enhancement of GDP firing. Panel A is the time course showing the average GDP firing frequency for five cells. Each column represents the number of GDPs recorded in 1 min. The dotted line represents the mean GDP frequency under control condition. Bath application of H7 inhibited GDP occurrence and blocked gp120-associated enhancement of GDPs. The average frequencies taken from control, during applications of H7 and H7 + gp120, and washout period are presented as a bar graph (B). Note gp120 failed to enhance GDPs in the presence of H7 in the perfusate. Panels C and D illustrate that activation of adenylyl cyclase by forskolin mimicked the effect of gp120 on GDPs, suggesting the possible involvement of PKA in gp120 enhancement of GDPs. A comparison of average GDP frequencies taken during washout periods following bath application of gp120, H7 + gp120 and forskolin are shown in panel E. Note that H7 blocked and forskolin mimicked the effects of gp120 on GDPs. $*P < 0.05$; $**P < 0.01$.

gp120-induced enhancement of GDP frequency was blocked by a highly specific CXCR4 receptor antagonist, T140, indicating the involvement of CXCR4 receptors in the gp120-associated increase of GDP frequency. Application of SDF-1α, the only ligand for CXCR4, mimicked the effects of gp120 on GDPs, further supporting our finding that gp120 increases GDP occurrence through CXCR4 receptors. The involvement of PKA/PKC in gp120-induced enhancement of GDPs was confirmed by bath application of H7, an antagonist for PKA/PKC.

HIV-1 gp120 is toxic to neurons and causes neural cell death at very low concentrations *in vitro* (Brenneman *et al.*, 1988; Dreyer *et al.*, 1990). In HIV-1-infected brain, gp120 is shed from virions and has the potential to diffuse and interact directly with surrounding and distant neural cells through activation of CXCR4 receptors (Hesselgesser *et al.*, 1998; Meucci *et al.*, 1998; Acquas *et al.*, 2004; Bachis & Mocchetti, 2004), or by stimulating uninfected macrophage-glial cells to release toxins that act indirectly on local and distant neural cells, or both. Treatment of human or rat neurons in culture with gp120 leads to neuronal apoptosis (Bachis & Mocchetti, 2004; Brenneman *et al.*, 1988; Meucci *et al.*, 1996) and intracerebroventricular injection of gp120 in rats produces apoptotic neuronal death *in vivo* (Bagetta *et al.*, 1996b; Acquas *et al.*, 2004). Transgenic mice expressing the HIV-1 gp120 manifest a spectrum of neuronal and glial changes resembling abnormalities in brains of HIV-1-infected humans and the severity of damage correlated positively with the brain levels of gp120 expression (Toggas *et al.*, 1994). Our results showed that gp120 enhances GDP frequency without significant influence on neuronal resting membrane potential, membrane input resistance and spontaneous EPSPs. This suggests that gp120 most likely alters GDP frequency by acting on other cellular elements in the hippocampus

such as interneurons, astrocytes and/or microglia that also express CXCR4 receptors (Tanabe *et al.*, 1997; Klein *et al.*, 1999). A hypothetical model of gp120-induced enhancement of GDP frequency is shown in Fig. 7.

GDPs are network-driven membrane oscillations characterized by recurrent membrane depolarization with superimposed fast action potentials. They are large synaptic events recorded in rat hippocampal slices between postnatal days P0 to P10 (Ben-Ari *et al.*, 1989). GDPs are synchronized locally within a temporal frame of several hundreds of milliseconds and recur at a frequency of approximately 0.1 Hz (Ben-Ari, 2001; Kasyanov *et al.*, 2004). They constitute the first synaptic pattern observed in the connections that are established around the time of birth with an extensive growth at the second postnatal week (Gaiarsa *et al.*, 1992; Gomez-Di Cesare *et al.*, 1997). During this period of intensive growth, GDPs provide most of the ongoing activity in pyramidal neurons and interneurons (Khazipov *et al.*, 1997). Because GDPs resulting from the excitatory effects of GABA can increase the levels of $[Ca^{2+}]_i$ through voltage-gated Ca^{2+} channels and NMDA receptor channels (Leinekugel *et al.*, 1995; Leinekugel *et al.*, 1997) and because application of gp120 increases the levels of $[Ca^{2+}]_i$ the persistent increase of GDPs mediated by gp120 may cause neuronal damage as a result of excessive increase of $[Ca^{2+}]_i$, leading to retardation of brain development and deterioration in cognitive function. Interestingly, hippocampal-dependent integrative functions – learning and memory – emerge later at the end of the first postnatal month (Altman *et al.*, 1973; Rudy & Stadler-Morris, 1987), suggesting that GDPs occur at an early period during which the hippocampus does not perform the integrative functions. Thus, the persistent increase of GDP frequency by gp120 during the first postnatal week may disturb the subsequent synaptogenesis and hippocampal integrative functions such as learning and memory (Ben-Ari, 2001), leading to cognitive decline as seen in paediatric AIDS patients with HE.

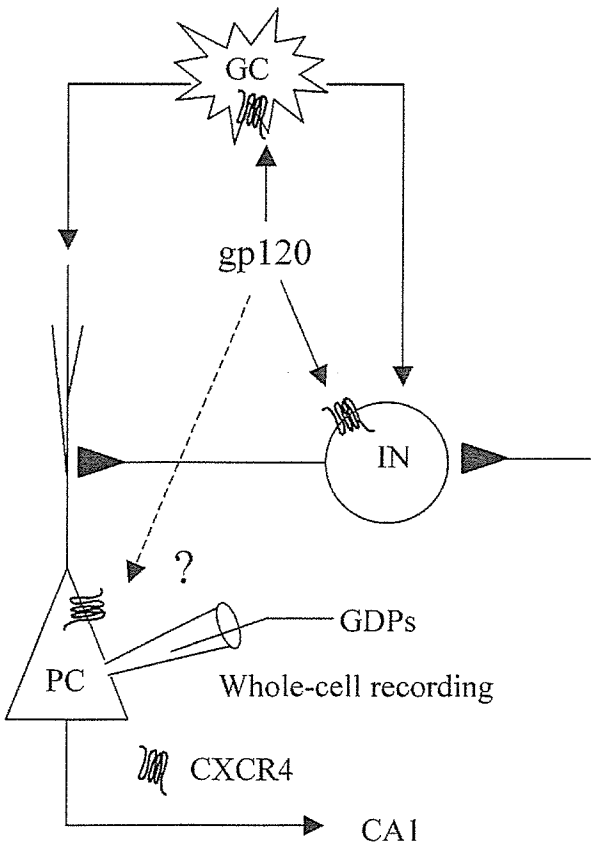

FIG. 7. A hypothetical model of gp120-induced enhancement of GDP frequency. Gp120 may act on CXCR4 receptors expressed on interneurons (IN) and increase GABA release. Gp120 may also act on glial cell (GC) CXCR4 receptors and enhance glial cell secretion of cytokines/chemokines and other bioactive molecules. These bioactive substances may target interneurons and/or CA3 pyramidal cells (PC) and up-regulate interneuron secretion of GABA and/or enhance the sensitivity of CA3 pyramidal cells to GABA, or both.

In the immature brain, transient elevations of $[Ca^{2+}]_i$ are important in many aspects of development at the network level. These include proliferation (LoTurco *et al.*, 1995), neuronal migration (Komuro & Rakic, 1996), and motility of axonal and dendritic growth cones (Kater *et al.*, 1988). Many of these Ca^{2+}-dependent processes require repeated, periodic changes of $[Ca^{2+}]_i$. As the GDPs are recurrent synaptic events that involve large populations of neurons (Garaschuk *et al.*, 1998; Garaschuk *et al.*, 2000), they may represent a prime candidate to promote neuronal development and to 'synchronize' development over large neuronal populations. However, a sustained elevation of $[Ca^{2+}]_i$ may cause neural cell damage. It has been shown in rat primary hippocampal neuronal cultures that gp120 produced a delayed onset, long-lasting intracellular Ca^{2+} oscillation (Lo *et al.*, 1992) and elevated intracellular free Ca^{2+} levels (Lo *et al.*, 1992; Pandey & Bolsover, 2000). We have also observed that gp120 produced a sustained increase of $[Ca^{2+}]_i$ in primary rat hippocampal-cortical neuronal cultures (Fig. 3). Consistent with these previous observations, we found that gp120 produced a delayed onset in the increase of GDP frequency. As membrane depolarization during GDPs increases $[Ca^{2+}]_i$ through the activation of voltage-dependent Ca^{2+} channels in interneurons and pyramidal cells in the hippocampus (Leinekugel *et al.*, 1995), the long-lasting enhancement of GDP frequency induced by gp120 may result in excessive increase of $[Ca^{2+}]_i$, leading to neuronal dysfunction and/or death. Thus, elevation of $[Ca^{2+}]_i$ in the neurons as a result of gp120-induced increase of GDP occurrence may play an important role in the pathogenesis of HIV-1-associated neurological symptoms seen in infants and children.

Chemokine receptor CXCR4, a coreceptor for HIV-1 entry into the target cells, is expressed in human and rat hippocampal glial and neuronal cells (Lavi *et al.*, 1997; Meucci *et al.*, 1998; Banisadr *et al.*, 2002). The functional significance of CXCR4 expression in hippocampal neurons is not fully understood. It has been shown that the brains of mouse embryos without CXCR4 receptors have a severe abnormality in the development of cerebellar morphology (Ma *et al.*, 1998; Zou *et al.*, 1998). Activation of neuronal CXCR4 receptors by a physiological agonist, SDF-1α, modulates synaptic transmission in developing rat cerebellum (Limatola *et al.*, 2000). In contrast to its physiological role, CXCR4 has been shown to play a key role in mediating gp120 cytotoxicity in both immune cells (Herbein *et al.*, 1998) and neurons (Meucci *et al.*, 2000), even in the absence of the cell surface glycoprotein CD4 (Hesselgesser *et al.*, 1998). Activation of CXCR4 triggers a transient increase of $[Ca^{2+}]_i$ (Zheng *et al.*, 1999), which is believed to participate in gp120 neurotoxicity (Haughey & Mattson, 2002). Thus, the CXCR4 has been speculated as the primary target of gp120 in mediating neuronal toxicity (Bachis & Mocchetti, 2004). We found that bath application of T140, a CXCR4 receptor antagonist, blocked gp120-induced enhancement of GDP firing frequency. This blockade indicates the involvement of the chemokine receptor, CXCR4, in gp120 enhancement of GDP firing. This finding is further supported by experimental results that bath application of the only CXCR4 receptor agonist, SDF-1α, mimicked the effects of gp120 on GDPs. It is worth pointing out that SDF-1α decreased GDP frequency during the bath perfusion period, an effect that was not observed during bath application of gp120. The potential

mechanism(s) underlying this difference remains to be determined. It may result that SDF-1α and gp120 engage different mechanisms in stimulating and/or regulating GABA release following their binding to G-protein-coupled CXCR4 receptors expressed on interneurons, glial cells and/or CA3 pyramidal cells. It may also be the consequence that the glial cells, stimulated by gp120 or SDF-1α, release a different spectrum of cytokines and/or chemokines that influence GABA-mediated synaptic events or change the feature of 'pacemaker' cells in the immature hippocampus, or both.

Several groups have reported the effects of HIV-1 gp120 on signal transduction pathways in the CNS (Zorn *et al.*, 1990; Schneider-Schaulies *et al.*, 1992; Wyss-Coray *et al.*, 1996). Gp120 activates PKC (Zorn *et al.*, 1990) and induces PKC translocation differentially in rat primary neuronal cultures(Ushijima *et al.*, 1993). Based on these observations, we reasoned that gp120 may enhance GDP firing through PKC. Our results showed that gp120-induced enhancement of GDP occurrence was blocked by a PKC antagonist, H7, demonstrating the involvement of PKC in the gp120-induced increase of GDPs. In addition, we found that the adenylyl cyclase stimulator forskolin mimicked the effects of gp120 on GDPs, suggesting the possible involvement of cAMP-dependent kinase in gp120-associated signalling as well. Taken together, our results revealed that HIV-1 gp120 enhances GDPs via the chemokine receptor, CXCR4, in neonatal rat hippocampal slices and this enhancement was mediated through PKA/PKC-dependent pathway.

Acknowledgements

We are grateful to NIH AIDS Research & Reference Reagent Program for providing HIV-1 gp120 for this study. We thank Drs Howard E. Gendelman and Mark Thomas, Ms Elizabeth Irvine and Ms Robin Taylor for reading the manuscript. This work was supported by an NIH grant R01 NS41862.

Abbreviations

EPSPs, excitatory postsynaptic potentials; GDPs, giant depolarizing potentials; HAD, HIV-1-associated dementia; HE, HIV-1-associated encephalopathy; HIV-1, human immunodeficiency virus type one; MPs, mononuclear phagocytes; PKA, cAMP-dependent protein kinase; PKC, protein kinase C.

References

Acquas, E., Bachis, A., Nosheny, R.L., Cernak, I. & Mocchetti, I. (2004) Human immunodeficiency virus type 1 protein gp120 causes neuronal cell death in the rat brain by activating caspases. *Neurotox. Res.*, **5**, 605–615.

Altman, J., Brunner, R.L. & Bayer, S.A. (1973) The hippocampus and behavioral maturation. *Behav. Biol.*, **8**, 557–596.

Ammann, A.J. (1994) Human immunodeficiency virus infection/AIDS in children: the next decade. *Pediatrics*, **93**, 930–935.

Asensio, V.C. & Campbell, I.L. (1999) Chemokines in the CNS: plurifunctional mediators in diverse states. *TINS*, **22**, 504–512.

Bachis, A. & Mocchetti, I. (2004) The chemokine receptor CXCR4 and not the *N*-methyl-D-aspartate receptor mediates gp120 neurotoxicity in cerebellar granule cells. *J. Neurosci. Res.*, **75**, 75–82.

Bagetta, G., Corasaniti, M.T., Aloe, L., Berliocchi, L., Costa, N., Finazzi-Agro, A. & Nistico, G. (1996a) Intracerebral injection of human immunodeficiency virus type 1 coat protein gp120 differentially affects the expression of nerve growth factor and nitric oxide synthase in the hippocampus of rat. *Proc. Natl Acad. Sci. USA*, **93**, 928–933.

Bagetta, G., Corasaniti, M.T., Malorni, W., Rainaldi, G., Berliocchi, L., Finazzi-Agro, A. & Nistico, G. (1996b) The HIV-1 gp120 causes ultrastructural changes typical of apoptosis in the rat cerebral cortex. *Neuroreport*, **7**, 1722–1724.

Banisadr, G., Fontanges, P., Haour, F., Kitabgi, P., Rostene, W. & Melik Parsadaniantz, S. (2002) Neuroanatomical distribution of CXCR4 in adult rat brain and its localization in cholinergic and dopaminergic neurons. *Eur. J. Neurosci.*, **16**, 1661–1671.

Bansal, A.K., Mactutus, C.F., Nath, A., Maragos, W., Hauser, K.F. & Booze, R.M. (2000) Neurotoxicity of HIV-1 proteins gp120 and Tat in the rat striatum. *Brain Res.*, **879**, 42–49.

Belman, A.L. (1994) HIV-1-Associated CNS Disease in Infants and Children. *Res. Publications Assoc. Res. Nerv. Ment. Dis.*, **72**, 289–310.

Belman, A.L., Diamond, G., Dickson, D., Horoupian, D., Llena, J., Lantos, G. & Rubinstein, A. (1988) Pediatric acquired immunodeficiency syndrome. Neurologic syndromes. *Am. J. Dis. Child*, **142**, 29–35.

Belman, A.L., Iyer, M., Coyle, P.K. & Dattwyler, R. (1993) Neurologic manifestations in children with North American Lyme disease. *Neurology*, **43**, 2609–2614.

Ben-Ari, Y. (2001) Developing networks play a similar melody. *TINS*, **24**, 353–360.

Ben-Ari, Y., Cherubini, E., Corradetti, R. & Gaiarsa, J.L. (1989) Giant synaptic potentials in immature rat CA3 hippocampal neurones. *J. Physiol.*, **416**, 303–325.

Brenneman, D.E., Westbrook, G.L., Fitzgerald, S.P., Ennist, D.L., Elkins, K.L., Ruff, M.R. & Pert, C.B. (1988) Neuronal cell killing by the envelope protein of HIV and its prevention by vasoactive intestinal peptide. *Nature*, **335**, 639–642.

Croitoru-Lamoury, J., Guillemin, G.J., Boussin, F.D., Mognetti, B., Gigout, L.I., Cheret, A., Vaslin, B., Le Grand, R., Brew, B.J. & Dormont, D. (2003) Expression of chemokines and their receptors in human and simian astrocytes: evidence for a central role of TNF alpha and IFN gamma in CXCR4 and CCR5 modulation. *Glia*, **41**, 354–370.

Dawson, V.L., Dawson, T.M., Uhl, G.R. & Snyder, S.H. (1993) Human immunodeficiency virus type 1 coat protein neurotoxicity mediated by nitric oxide in primary cortical cultures. *Proc. Natl Acad. Sci. USA*, **90**, 3256–3259.

Dreyer, E.B., Kaiser, P.K., Offermann, J.T. & Lipton, S.A. (1990) HIV-1 coat protein neurotoxicity prevented by calcium channel antagonists. *Science*, **248**, 364–367.

Epstein, L.G., Sharer, L.R., Oleske, J.M., Connor, E.M., Goudsmit, J., Bagdon, L., Robert-Guroff, M. & Koenigsberger, M.R. (1986) Neurologic manifestations of human immunodeficiency virus infection in children. *Pediatrics*, **78**, 678–687.

Gaiarsa, J.L., Beaudoin, M. & Ben-Ari, Y. (1992) Effect of neonatal degranulation on the morphological development of rat CA3 pyramidal neurons: inductive role of mossy fibers on the formation of thorny excrescences. *J. Comp. Neurol.*, **321**, 612–625.

Garaschuk, O., Hanse, E. & Konnerth, A. (1998) Developmental profile and synaptic origin of early network oscillations in the CA1 region of rat neonatal hippocampus. *J. Physiol.*, **507**, 219–236.

Garaschuk, O., Linn, J., Eilers, J. & Konnerth, A. (2000) Large-scale oscillatory calcium waves in the immature cortex. *Nature Neurosci.*, **3**, 452–459.

Gendelman, H.E., Persidsky, Y., Ghorpade, A., Limoges, J., Stins, M., Fiala, M. & Morrisett, R. (1997) The neuropathogenesis of the AIDS dementia complex. *Aids*, **11**, S35–S45.

Gomez-Di Cesare, C.M., Smith, K.L., Rice, F.L. & Swann, J.W. (1997) Axonal remodeling during postnatal maturation of CA3 hippocampal pyramidal neurons. *J. Comp. Neurol.*, **384**, 165–180.

Haughey, N.J. & Mattson, M.P. (2002) Calcium dysregulation and neuronal apoptosis by the HIV-1 proteins Tat and gp120. *J. Acquir. Immune Defic. Syndr.*, **31**, S55–S61.

Herbein, G., Mahlknecht, U., Batliwalla, F., Gregersen, P., Pappas, T., Butler, J., O'Brien, W.A. & Verdin, E. (1998) Apoptosis of CD8+ T cells is mediated by macrophages through interaction of HIV gp120 with chemokine receptor CXCR4. *Nature*, **395**, 189–194.

Hesselgesser, J., Taub, D., Baskar, P., Greenberg, M., Hoxie, J., Kolson, D.L. & Horuk, R. (1998) Neuronal apoptosis induced by HIV-1 gp120 and the chemokine SDF-1 alpha is mediated by the chemokine receptor CXCR4. *Curr. Biol.*, **8**, 595–598.

Hill, J.M., Mervis, R.F., Avidor, R., Moody, T.W. & Brenneman, D.E. (1993) HIV envelope protein-induced neuronal damage and retardation of behavioral development in rat neonates. *Brain Res.*, **603**, 222–233.

Horuk, R., Martin, A.W., Wang, Z., Schweitzer, L., Gerassimides, A., Guo, H., Lu, Z., Hesselgesser, J., Perez, H.D., Kim, J., Parker, J., Hadley, T.J. & Peiper, S.C. (1997) Expression of chemokine receptors by subsets of neurons in the central nervous system. *J. Immunol.*, **158**, 2882–2890.

Huang, M.B. & Bond, V.C. (2000) Involvement of protein kinase C in HIV-1 gp120-induced apoptosis in primary endothelium. *J. Acquir. Immune Defic. Syndr.*, **25**, 375–389.

Kasyanov, A.M., Safiulina, V.F., Voronin, L.L. & Cherubini, E. (2004) GABA-mediated giant depolarizing potentials as coincidence detectors for enhancing synaptic efficacy in the developing hippocampus. *Proc. Natl Acad. Sci. USA*, **101**, 3967–3972.

Kater, S.B., Mattson, M.P., Cohan, C. & Connor, J. (1988) Calcium regulation of the neuronal growth cone. *TINS*, **11**, 315–321.

Kaul, M., Garden, G.A. & Lipton, S.A. (2001) Pathways to neuronal injury and apoptosis in HIV-associated dementia. *Nature*, **410**, 988–994.

Khazipov, R., Leinekugel, X., Khalilov, I., Gaiarsa, J.L. & Ben-Ari, Y. (1997) Synchronization of GABAergic interneuronal network in CA3 subfield of neonatal rat hippocampal slices. *J. Physiol.*, **498**, 763–772.

Klein, R.S., Williams, K.C., Alvarez-Hernandez, X., Westmoreland, S., Force, T., Lackner, A.A. & Luster, A.D. (1999) Chemokine receptor expression and signaling in macaque and human fetal neurons and astrocytes: implications for the neuropathogenesis of AIDS. *J. Immunol.*, **163**, 1636–1646.

Komuro, H. & Rakic, P. (1996) Intracellular Ca^{2+} fluctuations modulate the rate of neuronal migration. *Neuron*, **17**, 275–285.

Lannuzel, A., Lledo, P.M., Lamghitnia, H.O., Vincent, J.D. & Tardieu, M. (1995) HIV-1 envelope proteins gp120 and gp160 potentiate NMDA-induced $[Ca^{2+}]_i$ increase, alter $[Ca^{2+}]_i$ homeostasis and induce neurotoxicity in human embryonic neurons. *Eur. J. Neurosci.*, **7**, 2285–2293.

Lavi, E., Kolson, D.L., Ulrich, A.M., Fu, L. & Gonzalez-Scarano, F. (1998) Chemokine receptors in the human brain and their relationship to HIV infection. *J. Neurovirol.*, **4**, 301–311.

Lavi, E., Strizki, J.M., Ulrich, A.M., Zhang, W., Fu, L., Wang, Q., O'Connor, M., Hoxie, J.A. & Gonzalez-Scarano, F. (1997) CXCR-4 (Fusin), a co-receptor for the type 1 human immunodeficiency virus (HIV-1), is expressed in the human brain in a variety of cell types, including microglia and neurons. *Am. J. Pathol.*, **151**, 1035–1042.

Leinekugel, X., Medina, I., Khalilov, I., Ben-Ari, Y. & Khazipov, R. (1997) Ca^{2+} oscillations mediated by the synergistic excitatory actions of GABA(A) and NMDA receptors in the neonatal hippocampus. *Neuron*, **18**, 243–255.

Leinekugel, X., Tseeb, V., Ben-Ari, Y. & Bregestovski, P. (1995) Synaptic GABAA activation induces Ca^{2+} rise in pyramidal cells and interneurons from rat neonatal hippocampal slices. *J. Physiol.*, **487**, 319–329.

Limatola, C., Giovannelli, A., Maggi, L., Ragozzino, D., Castellani, L., Ciotti, M.T., Vacca, F., Mercanti, D., Santoni, A. & Eusebi, F. (2000) SDF-1alpha-mediated modulation of synaptic transmission in rat cerebellum. *Eur. J. Neurosci.*, **12**, 2497–2504.

Lo, T.M., Fallert, C.J., Piser, T.M. & Thayer, S.A. (1992) HIV-1 envelope protein evokes intracellular calcium oscillations in rat hippocampal neurons. *Brain Res.*, **594**, 189–196.

LoTurco, J.J., Owens, D.F., Heath, M.J., Davis, M.B. & Kriegstein, A.R. (1995) GABA and glutamate depolarize cortical progenitor cells and inhibit DNA synthesis. *Neuron*, **15**, 1287–1298.

Ma, Q., Jones, D., Borghesani, P.R., Segal, R.A., Nagasawa, T., Kishimoto, T., Bronson, R.T. & Springer, T.A. (1998) Impaired B-lymphopoiesis, myelopoiesis, and derailed cerebellar neuron migration in CXCR4- and SDF-1-deficient mice. *Proc. Natl Acad. Sci. USA*, **95**, 9448–9453.

Medina, I., Ghose, S. & Ben-Ari, Y. (1999) Mobilization of intracellular calcium stores participates in the rise of $[Ca^{2+}]_i$ and the toxic actions of the HIV coat protein GP120. *Eur. J. Neurosci.*, **11**, 1167–1178.

Meucci, O., Fatatis, A., Holzwarth, J.A. & Miller, R.J. (1996) Developmental regulation of the toxin sensitivity of Ca(2+)-permeable AMPA receptors in cortical glia. *J. Neurosci.*, **16**, 519–530.

Meucci, O., Fatatis, A., Simen, A.A., Bushell, T.J., Gray, P.W. & Miller, R.J. (1998) Chemokines regulate hippocampal neuronal signaling and gp120 neurotoxicity. *Proc. Natl Acad. Sci. USA*, **95**, 14500–14505.

Meucci, O., Fatatis, A., Simen, A.A. & Miller, R.J. (2000) Expression of CX3CR1 chemokine receptors on neurons and their role in neuronal survival. *Proc. Natl Acad. Sci. USA*, **97**, 8075–8080.

Meucci, O. & Miller, R.J. (1996) gp120-induced neurotoxicity in hippocampal pyramidal neuron cultures: protective action of TGF-beta1. *J. Neurosci.*, **16**, 4080–4088.

Mintz, M. & Epstein, L.G. (1992) Neurologic manifestations of pediatric acquired immunodeficiency syndrome: clinical features and therapeutic approaches. *Semin. Neurol.*, **12**, 51–56.

Nath, A. (2002) Human immunodeficiency virus (HIV) proteins in neuropathogenesis of HIV dementia. *J. Infect. Dis.*, **186**, S193–S198.

Pandey, V. & Bolsover, S.R. (2000) Immediate and neurotoxic effects of HIV protein gp120 act through CXCR4 receptor. *Biochem. Biophys. Res. Comm.*, **274**, 212–215.

Rudy, J.W. & Stadler-Morris, S. (1987) Development of interocular equivalence in rats trained on a distal-cue navigation task. *Behav. Neurosci.*, **101**, 141–143.

Schneider-Schaulies, J., Schneider-Schaulies, S., Brinkmann, R., Tas, P., Halbrugge, M., Walter, U., Holmes, H.C. & Ter Meulen, V. (1992) HIV-1 gp120 receptor on CD4-negative brain cells activates a tyrosine kinase. *Virology*, **191**, 765–772.

Tamamura, H. & Fujii, N. (2004) Two orthogonal approaches to overcome multi-drug resistant HIV-1s: development of protease inhibitors and entry inhibitors based on CXCR4 antagonists. *Curr. Drug Targets Infect. Disord.*, **4**, 103–110.

Tanabe, S., Heesen, M., Berman, M.A., Fischer, M.B., Yoshizawa, I., Luo, Y. & Dorf, M.E. (1997) Murine astrocytes express a functional chemokine receptor. *J. Neurosci.*, **17**, 6522–6528.

Tardieu, M., Le Chenadec, J., Persoz, A., Meyer, L., Blanche, S. & Mayaux, M.J. (2000) HIV-1-related encephalopathy in infants compared with children and adults. French Pediatric HIV Infection Study and the SEROCO Group. *Neurology*, **54**, 1089–1095.

Toggas, S.M., Masliah, E., Rockenstein, E.M., Rall, G.F., Abraham, C.R. & Mucke, L. (1994) Central nervous system damage produced by expression of the HIV-1 coat protein gp120 in transgenic mice. *Nature*, **367**, 188–193.

Ushijima, H., Ando, S., Kunisada, T., Schroder, H.C., Klocking, H.P., Kijjoa, A. & Muller, W.E. (1993) HIV-1 gp120 and NMDA induce protein kinase C translocation differentially in rat primary neuronal cultures. *J. Acquir. Immune Defic. Syndr.*, **6**, 339–343.

Vallat, A.V., De Girolami, U., He, J., Mhashilkar, A., Marasco, W., Shi, B., Gray, F., Bell, J., Keohane, C., Smith, T.W. & Gabuzda, D. (1998) Localization of HIV-1 co-receptors CCR5 and CXCR4 in the brain of children with AIDS. *Am. J. Pathol.*, **152**, 167–178.

Wyss-Coray, T., Masliah, E., Toggas, S.M., Rockenstein, E.M., Brooker, M.J., Lee, H.S. & Mucke, L. (1996) Dysregulation of signal transduction pathways as a potential mechanism of nervous system alterations in HIV-1 gp120 transgenic mice and humans with HIV-1 encephalitis. *J. Clin. Invest.*, **97**, 789–798.

Zheng, J., Thylin, M.R., Ghorpade, A., Xiong, H., Persidsky, Y., Cotter, R., Niemann, D., Che, M., Zeng, Y.C., Gelbard, H.A., Shepard, R.B., Swartz, J.M. & Gendelman, H.E. (1999) Intracellular CXCR4 signaling, neuronal apoptosis and neuropathogenic mechanisms of HIV-1-associated dementia. *J. Neuroimmunol.*, **98**, 185–200.

Zorn, N.E., Weill, C.L. & Russell, D.H. (1990) The HIV protein, GP120, activates nuclear protein kinase C in nuclei from lymphocytes and brain. *Biochem. Biophys. Res. Comm.*, **166**, 1133–1139.

Zou, Y.R., Kottmann, A.H., Kuroda, M., Taniuchi, I. & Littman, D.R. (1998) Function of the chemokine receptor CXCR4 in haematopoiesis and in cerebellar development. *Nature*, **393**, 595–599.

Development of a linear type of low molecular weight CXCR4 antagonists based on T140 analogs†

Hirokazu Tamamura,*[a] Hiroshi Tsutsumi,[a] Hiroyuki Masuno,[a] Satoko Mizokami,[b] Kenichi Hiramatsu,[b] Zixuan Wang,[c] John O. Trent,[d] Hideki Nakashima,[e] Naoki Yamamoto,[f,g] Stephen C. Peiper[c] and Nobutaka Fujii*[b]

Received 14th March 2006, Accepted 24th April 2006
First published as an Advance Article on the web 12th May 2006
DOI: 10.1039/b603818b

A linear type of several low molecular weight CXCR4 antagonists were developed based on T140 analogs, which were previously found to be strong CXCR4 antagonists that block X4-HIV-1 entry and have inhibitory activities against cancer metastasis/progression and rheumatoid arthritis.

Introduction

A system of a chemokine receptor, CXCR4, and its endogenous ligand, stromal cell-derived factor-1 (SDF-1/CXCL12), has multiple important functions in normal physiology involving the migration of progenitors during embryologic development of the cardiovascular, hemopoietic and central nervous systems.[1] The CXCL12/CXCR4 system has been also recognized to be involved in several pathologic conditions, such as HIV infection,[2] cancer metastasis/progression[3] and rheumatoid arthritis (RA).[4] First, CXCR4 was identified as a co-receptor that is used in the entry of T cell line-tropic (X4-) HIV-1 into T cells.[2] Second, it is found that the CXCL12/CXCR4 system is involved in the metastasis of several types of cancers, including breast cancer, pancreatic cancer, melanoma, prostate cancer, kidney cancer, neuroblastoma, non-Hodgkin's lymphoma, lung cancer, ovarian cancer, multiple myeloma, chronic lymphocytic leukemia, acute lymphoblastic leukemia and malignant brain tumor,[3] and that this system might determine the metastatic destination of tumor cells. For instance, Müller *et al.* reported that CXCR4 is highly expressed in human breast cancer cells, while CXCL12 is highly expressed in lymph nodes, bone marrow, lung and liver, which represent the primary metastatic destinations of breast cancer, and that breast cancer metastasis can be significantly inhibited by neutralization using anti-CXCR4 antibodies in mice.[3a] Third, Nanki *et al.* reported that the memory T cells highly express CXCR4 and the concentration of CXCL12 is extremely high in the synovium of RA patients, and that CXCL12 stimulates migration of the memory T cells and inhibits T cell apoptosis followed by T cell accumulation in the RA synovium.[4a] Taken together, CXCR4 is thought to represent an important therapeutic target.[5] Thus, several antagonists directed against CXCR4 have been developed. We previously found a 14-mer peptide, T140, which specifically antagonizes CXCR4,[6] and that Arg[2], L-3-(2-naphthyl)alanine (Nal)[3], Tyr[5] and Arg[14] constitute the biologically critical residues of T140 (Fig. 1).[7] Recently, its potent analogs, 4F-benzoyl-TN14003 and 4F-benzoyl-TE14011, possessing increased stability in serum and liver homogenate, were developed by introduction of a *p*-fluorobenzoyl group, which was defined as a new pharmacophore, into the *N*-terminus.[8] 4F-benzoyl-TN14003 and 4F-benzoyl-TE14011 showed strong anti-HIV activity *in vitro*, anti-metastatic activity against breast cancer[3b] and melanoma[3g] and anti-RA activity in experimental model mice.[4b] Furthermore, T140-related analogs exhibited significant inhibition against CXCL12-induced migration/activation/invasion of small-cell lung cancer cells,[3h] acute lymphoblastic leukemia cells[3e] and pancreatic cancer cells[3c,f] *in vitro*. Molecular-size reduction of T140 based on the above four critical residues (Arg × 2, Nal and Tyr) led to discovery of a low molecular weight CXCR4 antagonist with a cyclic pentapeptide template, FC131.[9] In this paper, identification of the enhanced pharmacophore involving an electron-deficient aromatic ring at the *N*-terminus of 4F-benzoyl-TN14003 and 4F-benzoyl-TE14011, such as a *p*-fluorobenzoyl or *p*-trifluoromethylbenzoyl moiety, prompted us to develop novel linear-type low molecular weight CXCR4 antagonists. By combining substructure units of

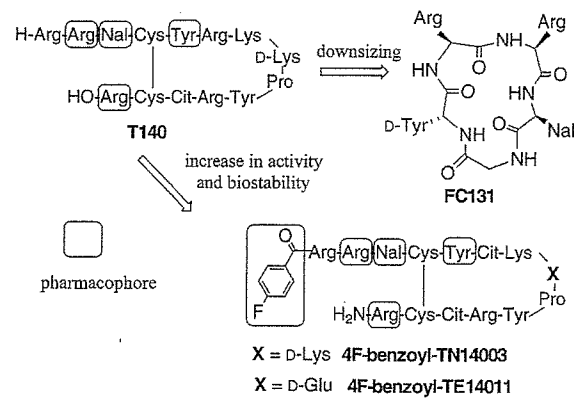

Fig. 1 Development of bio-stable CXCR4 antagonists, 4F-benzoyl-TN14003 and 4F-benzoyl-TE14011, and a downsized antagonist, FC131. Nal = L-3-(2-naphthyl)alanine, Cit = L-citrulline.

[a]*Institute of Biomaterials and Bioengineering, Tokyo Medical and Dental University, Chiyoda-ku, Tokyo 101-0062, Japan. E-mail: tamamura.mr@tmd.ac.jp; Fax: 81 3 5280 8039; Tel: 81 3 5280 8036*
[b]*Graduate School of Pharmaceutical Sciences, Kyoto University, Sakyo-ku, Kyoto 606-8501, Japan. E-mail: nfujii@pharm.kyoto-u.ac.jp; Fax: 81 75 753 4570; Tel: 81 75 753 4551*
[c]*Medical College of Georgia Augusta, GA 30912, USA*
[d]*James Graham Brown Cancer Center, University of Louisville, Louisville, KY 40202, USA*
[e]*St. Marianna University, School of Medicine, Miyamae-ku, Kawasaki 216-8511, Japan*
[f]*AIDS Research Center, National Institute of Infectious Diseases, Shinjuku-ku, Tokyo 162-8640, Japan*
[g]*Graduate School, Tokyo Medical and Dental University, Bunkyo-ku, Tokyo 113-8519, Japan*

† Electronic supplementary information (ESI) available: experimental and characterization data (MS) of novel synthetic compounds. See DOI: 10.1039/b603818b

the above four critical residues (Arg × 2, Nal and Tyr) that were used in the development of FC131, in addition to the above electron-deficient aromatic ring, several compounds were designed and synthesized.

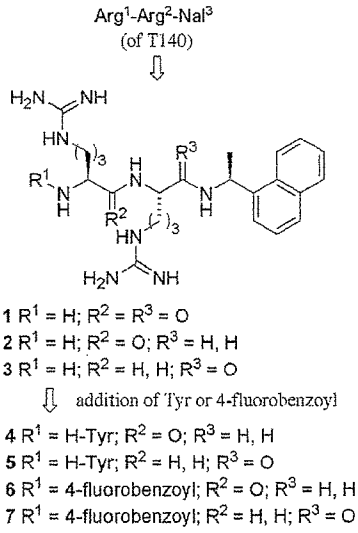

Fig. 2 Development of tri- and tetrapeptide mimetics with CXCR4-antagonistic activity.

Biological results and discussion

Biological activities of the present synthetic compounds were evaluated by two assays: the 3-(4, 5-dimethylthiazol-2-yl)-2, 5-diphenyltetrazolium bromide (MTT) assay based on the inhibition of X4-HIV-1 (HIV-1_{IIIB})-induced cytopathogenicity in MT-4 cells by test compounds (anti-HIV activity)[10] and a blocking assay based on displacement of CXCL12 binding to CXCR4 by test compounds (binding affinity for CXCR4).[11] Initially, three tripeptide mimetics containing amide bonds and/or reduced amide bonds, **1**–**3** were designed based on the sequence of Arg¹–Arg²–Nal³ in the *N*-terminal region of T140 (Fig. 1 and 2) and synthesized using solution-phase techniques involving amide bond-forming condensation and reductive amination reactions. In this study, (*S*)-(−)-1-(1-naphthyl)ethylamide, which was used in another CXCR4 antagonist KRH-1636,[12] was introduced with the view to enhancement of biostability. Compounds **2** and **3** showed significant anti-HIV activity, while compound **1** did not exhibit activity until the 100 μM concentration, suggesting that a reduced amide bond possessing the conformational flexibility might be more suitable for the interaction of CXCR4 (Table 1).

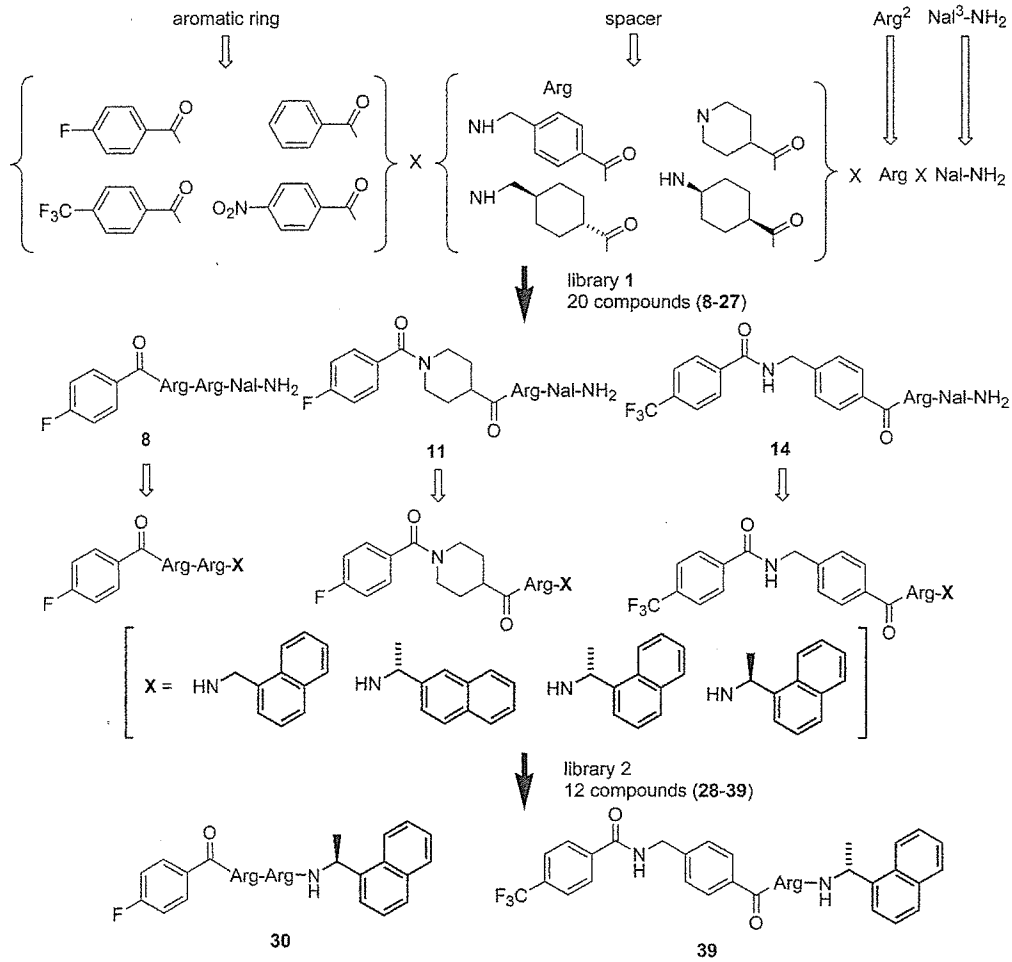

Fig. 3 Design of tripeptide library containing three pharmacophores of the *N*-terminal region of 4F-benzoyl-TN14003 and 4F-benzoyl-TE14011 (aromatic ring, Arg² and Nal³) and the development of new leads.

Table 1 Cytotoxicity, anti-HIV activity and inhibitory activity against CXCL12 binding to CXCR4 of the synthetic compounds

Compound	$CC_{50}/\mu M^a$	$EC_{50}/\mu M^b$	$IC_{50}/\mu M^c$
1	>100	>100	0.32–1
2	>100	52	0.32–1
3	>100	46	0.32–1
4	>100	22	0.090
5	>100	26	0.30
6	>100	11	0.32–1
7	>100	1.7	>1
8	>100	45	0.30
11	>100	7.7	>1
14	>100	6.0	>1
30	>100	61	>1
39	66	7.4	>1
FC131	>100	0.073	0.0032
T140	>10	0.026	0.0045
AZT	>100	0.014	

[a] CC_{50} values are based on the reduction of the viability of mock-infected MT-4 cells. Since the cytotoxicity of T140 was previously evaluated as CC50 > 40 μM, further estimation at high concentrations was omitted in this study. [b] EC_{50} values are based on the inhibition of HIV-induced cytopathogenicity in MT-4 cells. [c] IC_{50} values are based on the inhibition of [^{125}I]-CXCL12 binding to CXCR4 transfectants of CHO cells. All data are the mean values for at least three independent experiments.

Thus, we synthesized two tetrapeptide mimetics, **4** and **5**, where a Tyr residue was added in the *N*-terminus of compounds **2** and **3**, respectively, based on the sequence of the FC131 sequence. Compounds **4** and **5** showed approximately twice stronger anti-HIV activity than compounds **2** and **3**, indicating that an *N*-terminal addition of a Tyr residue is effective for an increase in anti-HIV activity. Furthermore, compounds **4** and **5** exhibited stronger binding affinity for CXCR4, compared to compounds **1**–**3**. Next, we synthesized *p*-fluorobenzoylated tripeptide mimetics, **6** and **7**, based on the *N*-terminal sequence of 4F-benzoyl-TN14003 and 4F-benzoyl-TE14011. As a result, *p*-fluorobenzoylation caused an increase in anti-HIV activity. Compound **7** showed strong anti-HIV activity, suggesting that introduction of a reduced amide bond between two Arg residues is more suitable than that between Arg and naphthalenylethylamine. However, binding affinity of compound **7** for CXCR4 could not be exhibited until the 1 μM concentration, and compound **6** is weaker than compounds **4** and **5** in terms of binding affinity for CXCR4, although anti-HIV activity of compounds **6** and **7** is stronger than that of compounds **4** and **5**. This discrepancy might be caused by the difference between the interactive site of HIV and the binding site of CXCL12 on CXCR4.[13]

Since hit compounds with significant anti-HIV activity were found among several compounds that were synthesized using solution-phase techniques, we attempted to prepare more compounds by solid-phase synthesis: A tripeptide library containing three pharmacophores of the *N*-terminal region of 4F-benzoyl-TN14003 and 4F-benzoyl-TE14011 (aromatic ring, Arg^2 and Nal^3) and the *C*-terminal carboxy amide was designed (Fig. 3). Since Arg^1 is not an indispensable residue for high activity, it was replaced by several spacers involving conformationally constrained units, such as 4-piperidinecarboxylic acid and 4-(aminomethyl)benzoic acid. Use of this library involving 20 synthetic compounds, which was constructed by solid-phase peptide synthesis (Fig. 3, library 1), led to the discovery of lead compounds for anti-HIV agents, **11** and **14**, although these compounds did not show significant binding affinity for CXCR4 until the 1 μM concentration. Compound **8**, which contains Arg^1 based on the original 4F-benzoyl-TN14003 and 4F-benzoyl-TE14011 sequence, also exhibited moderate anti-HIV activity and significant CXCR4-binding affinity. These results suggest that Arg^1 can be replaced by conformationally restricted units in terms of anti-HIV activity. The other compounds that were contained in library 1 did not show significant anti-HIV activity until the 100 μM concentration.

Next, in due consideration of an increase in biostability, focused library of compounds with the *C*-terminal substituted amide was constructed based on the structures of compounds **8**, **11** and **14** by solid-phase techniques using Kenner's sulfonamide safety-catch linker[14] (Fig. 3, library 2): *C*-terminal Nal-amide of compounds **8**, **11** and **14** was replaced by several amides possessing various naphthalene units. The synthetic scheme for compound **39** is shown as a representative in Scheme 1. Compounds **30** and **39** showed moderate and strong anti-HIV activity, respectively, although each compound did not show significant CXCR4-binding affinity until the 1 μM concentration. Anti-HIV potency of compounds is not always in proportion to binding affinity for CXCR4, especially in case of these small compounds, since there is a significant difference between the interactive site of HIV and the binding site of CXCL12 on CXCR4. There is a great interest in this result: compound **39**, possessing (*R*)-(+)-1-(1-naphthyl)ethylamide in the *C*-terminus, is stronger than compound **38**, possessing (*S*)-(−)-1-(1-naphthyl)ethylamide in the

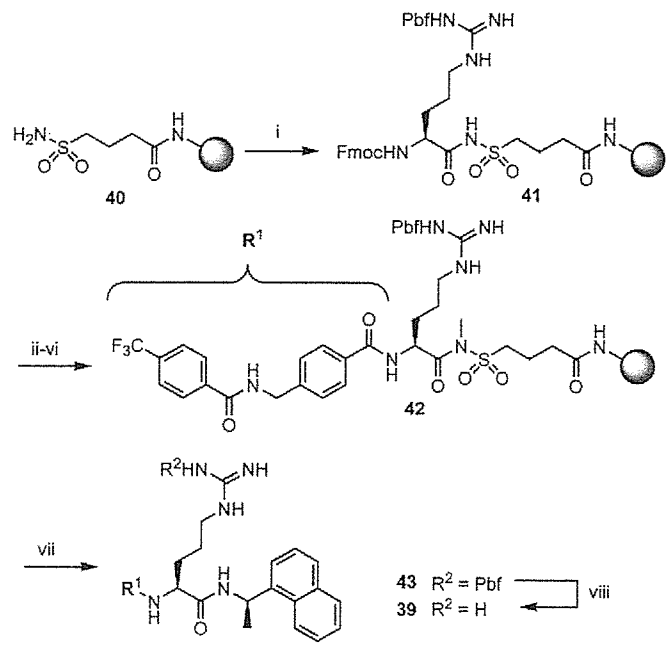

Scheme 1 Reagents: (i) Fmoc-Arg(Pbf)–OH, DIPEA, PyBOP, $CHCl_3$; (ii) 20% (v/v) piperidine–DMF; (iii) Fmoc-(4-aminomethyl)benzoic acid, DIPCDI, HOBt, DMF; (iv) 20% (v/v) piperidine–DMF; (v) 4-trifluoromethylbenzoic acid, DIPCDI, HOBt, DMF; (vi) $TMSCHN_2$, hexane, THF; (vii) (*R*)-(+)-1-(1-naphthyl)ethylamine, DMF, reflux; (viii) thioanisole, TFA; Pbf = 2,2,4,6,7-pentamethyl-dihydrobenzofuran-5-sulfonyl, DIPEA = *N*,*N*-diisopropylethylamine, PyBOP = benzotriazole-1-yl-oxy-tris-pyrrolidino-phosphonium hexafluorophosphate, DIPCDI = *N*,*N*-diisopropylcarbodiimide, HOBt = *N*-hydroxybenzotriazole.

C-terminus, which is a common structure unit with KRH-1636. Compound **39** is thought to be a useful lead possessing chemically modified *N*- and *C*-terminal ends. The other 10 compounds that were contained in library 2 did not show significant anti-HIV activity until the 100 μM concentration.

In summary, several compounds that were synthesized based on pharmacophores of T140 analogs showed significant anti-HIV activity and binding affinity for CXCR4. According to these results, two types of libraries based on the *N*-terminal region of 4F-benzoyl-TN14003 and 4F-benzoyl-TE14011 were constructed to find effective lead compounds. Linear-type low molecular weight compounds obtained in this study are thought to be useful leads for chemotherapy of AIDS, cancer and RA.

Acknowledgements

This work was supported in part by a 21st Century COE Program "Knowledge Information Infrastructure for Genome Science", a Grant-in-Aid for Scientific Research from the Ministry of Education, Culture, Sports, Science and Technology, Japan, the Japan Health Science Foundation, The Mochida Memorial Foundation for Medical and Pharmaceutical Research and Philip Morris USA Inc. and Philip Morris International.

Notes and references

1 (*a*) T. Nagasawa, H. Kikutani and T. Kishimoto, *Proc. Natl. Acad. Sci. U. S. A.*, 1994, **91**, 2305; (*b*) C. C. Bleul, M. Farzan, H. Choe, C. Parolin, I. Clark-Lewis, J. Sodroski and T. A. Springer, *Nature*, 1996, **382**, 829; (*c*) E. Oberlin, A. Amara, F. Bachelerie, C. Bessia, J.-L. Virelizier, F. Arenzana-Seisdedos, O. Schwartz, J.-M. Heard, I. Clark-Lewis, D. F. Legler, M. Loetscher, M. Baggiolini and B. Moser, *Nature*, 1996, **382**, 833; (*d*) K. Tashiro, H. Tada, R. Heilker, M. Shirozu, T. Nakano and T. Honjo, *Science*, 1993, **261**, 600.

2 Y. Feng, C. C. Broder, P. E. Kennedy and E. A. Berger, *Science*, 1996, **272**, 872.

3 (*a*) A. Müller, B. Homey, H. Soto, N. Ge, D. Catron, M. E. Buchanan, T. McClanahan, E. Murphy, W. Yuan, S. N. Wagner, J. L. Barrera, A. Mohar, E. Verastegui and A. Zlotnik, *Nature*, 2001, **410**, 50; (*b*) H. Tamamura, A. Hori, N. Kanzaki, K. Hiramatsu, M. Mizumoto, H. Nakashima, N. Yamamoto, A. Otaka and N. Fujii, *FEBS Lett.*, 2003, **550**, 79; (*c*) T. Koshiba, R. Hosotani, Y. Miyamoto, J. Ida, S. Tsuji, S. Nakajima, M. Kawaguchi, H. Kobayashi, R. Doi, T. Hori, N. Fujii and M. Imamura, *Clin. Cancer Res.*, 2000, **6**, 3530; (*d*) N. Tsukada, J. A. Burger, N. J. Zvaifler and T. J. Kipps, *Blood*, 2002, **99**, 1030; (*e*) J. Juarez, K. F. Bradstock, D. J. Gottlieb and L. J. Bendall, *Leukemia*, 2003, **17**, 1294; (*f*) T. Mori, R. Doi, M. Koizumi, E. Toyoda, S. S. Tulachan, D. Ito, K. Kami, T. Masui, K. Fujimoto, H. Tamamura, K. Hiramatsu, N. Fujii and M. Imamura, *Mol. Cancer Ther.*, 2004, **3**, 29; (*g*) M. Takenaga, H. Tamamura, K. Hiramatsu, N. Nakamura, Y. Yamaguchi, A. Kitagawa, S. Kawai, H. Nakashima, N. Fujii and R. Igarashi, *Biochem. Biophys. Res. Commun.*, 2004, **320**, 226; (*h*) M. Burger, A. Glodek, T. Hartmann, A. Schmitt-Graff, L. E. Silberstein, N. Fujii, T. J. Kipps and J. A. Burger, *Oncogene*, 2003, **22**, 8093.

4 (*a*) T. Nanki, K. Hayashida, H. S. El-Gabalawy, S. Suson, K. Shi, H. J. Girschick, S. Yavuz and P. E. Lipsky, *J. Immunol.*, 2000, **165**, 6590; (*b*) H. Tamamura, M. Fujisawa, K. Hiramatsu, M. Mizumoto, H. Nakashima, N. Yamamoto, A. Otaka and N. Fujii, *FEBS Lett.*, 2004, **569**, 99.

5 (*a*) H. Tamamura and N. Fujii, *Expert Opin. Ther. Targets*, 2005, **9**, 1267; (*b*) H. Tamamura, A. Otaka and N. Fujii, *Curr. HIV Res.*, 2005, **3**, 289.

6 H. Tamamura, Y. Xu, T. Hattori, X. Zhang, R. Arakaki, K. Kanbara, A. Omagari, A. Otaka, T. Ibuka, N. Yamamoto, H. Nakashima and N. Fujii, *Biochem. Biophys. Res. Commun.*, 1998, **253**, 877.

7 H. Tamamura, A. Omagari, S. Oishi, T. Kanamoto, N. Yamamoto, S. C. Peiper, H. Nakashima, A. Otaka and N. Fujii, *Bioorg. Med. Chem. Lett.*, 2000, **10**, 2633.

8 H. Tamamura, K. Hiramatsu, M. Mizumoto, S. Ueda, S. Kusano, S. Terakubo, M. Akamatsu, N. Yamamoto, J. O. Trent, Z. Wang, S. C. Peiper, H. Nakashima, A. Otaka and N. Fujii, *Org. Biomol. Chem.*, 2003, **1**, 3663.

9 N. Fujii, S. Oishi, K. Hiramatsu, T. Araki, S. Ueda, H. Tamamura, A. Otaka, S. Kusano, S. Terakubo, H. Nakashima, J. A. Broach, J. O. Trent, Z. Wang and S. C. Peiper, *Angew. Chem., Int. Ed.*, 2003, **42**, 3251.

10 H. Nakashima, M. Masuda, T. Murakami, Y. Koyanagi, A. Matsumoto, N. Fujii and N. Yamamoto, *Antimicrob. Agents Chemother.*, 1992, **36**, 1249.

11 J. M. Navenot, Z. X. Wang, J. O. Trent, J. L. Murray, Q. X. Hu, L. DeLeeuw, P. S. Moore, Y. Chang and S. C. Peiper, *J. Mol. Biol.*, 2001, **313**, 1181.

12 K. Ichiyama, S. Yokoyama-Kumakura, Y. Tanaka, R. Tanaka, K. Hirose, K. Bannai, T. Edamatsu, M. Yanaka, Y. Niitani, N. Miyano-Kurosaki, H. Takaku, Y. Koyanagi and N. Yamamoto, *Proc. Natl. Acad. Sci. U. S. A.*, 2003, **100**, 4185.

13 J. O. Trent, Z. Wang, J. L. Murray, W. Shao, H. Tamamura, N. Fujii and S. C. Peiper, *J. Biol. Chem.*, 2003, **278**, 47136.

14 (*a*) B. J. Backes, A. A. Virgilio and J. A. Ellman, *J. Am. Chem. Soc.*, 1996, **118**, 3055; (*b*) B. J. Backes and J. A. Ellman, *J. Org. Chem.*, 1999, **64**, 2322; (*c*) R. Ingenito, E. Bianchi, D. Fattori and A. Pessi, *J. Am. Chem. Soc.*, 1999, **121**, 11369.

Available online at www.sciencedirect.com
SCIENCE DIRECT®
Nuclear Medicine and Biology 33 (2006) 489–494
NUCLEAR MEDICINE — AND — BIOLOGY
www.elsevier.com/locate/nucmedbio

Development of a ^{111}In-labeled peptide derivative targeting a chemokine receptor, CXCR4, for imaging tumors

Hirofumi Hanaoka[a,b], Takahiro Mukai[c,d], Hirokazu Tamamura[a,e], Tomohiko Mori[c], Seigo Ishino[a], Kazuma Ogawa[a], Yasuhiko Iida[b], Ryuichiro Doi[c], Nobutaka Fujii[a], Hideo Saji[a,*]

[a]*Graduate School of Pharmaceutical Sciences, Kyoto University, Yoshida Shimoadachi-cho, Sakyo-ku, Kyoto 606-8501, Japan*
[b]*Graduate School of Medicine, Gunma University, Showa-machi, Maebashi 371-8511, Japan*
[c]*Graduate School of Medicine, Kyoto University, Shogoin Kawahara-cho, Sakyo-ku, Kyoto 606-8507, Japan*
[d]*Graduate School of Pharmaceutical Sciences, Kyushu University, Maidashi, Higashi-ku, Fukuoka 812-8582, Japan*
[e]*Institute of Biomaterials and Bioengineering, Tokyo Medical and Dental University, Chiyoda-ku, Tokyo 101-0062, Japan*

Received 7 October 2005; received in revised form 12 January 2006; accepted 12 January 2006

Abstract

The chemokine receptor CXCR4 is highly expressed in tumor cells and plays an important role in tumor metastasis. The aim of this study was to develop a radiopharmaceutical for the imaging of CXCR4-expressing tumors in vivo. Based on structure–activity relationships, we designed a 14-residue peptidic CXCR4 inhibitor, Ac-TZ14011, as a precursor for radiolabeled peptides. For ^{111}In-labeling, diethylenetriaminepentaacetic acid (DTPA) was attached to the side chain of D-Lys^{8} which is distant from the residues indispensable for the antagonistic activity. In-DTPA-Ac-TZ14011 inhibited the binding of a natural ligand, stromal cell-derived factor-1α, to CXCR4 in a concentration-dependent manner with an IC_{50} of 7.9 nM (Ac-TZ14011: 1.2 nM). In biodistribution experiments, more ^{111}In-DTPA-Ac-TZ14011 accumulated in the CXCR4-expressing tumor than in blood or muscle. Furthermore, the tumor-to-blood and tumor-to-muscle ratios were significantly reduced by coinjection of Ac-TZ14011, indicating a CXCR4-mediated accumulation in tumor. These findings suggested that ^{111}In-DTPA-Ac-TZ14011 would be a potential agent for the imaging of CXCR4 expression in metastatic tumors in vivo.

Keywords: CXCR4; Peptide radiopharmaceutical; Indium-111; Metastatic tumor

1. Introduction

Chemokines are a family of small proteins (8–14 kDa) that chemoattract leukocytes by binding to cell surface receptors, chemokine receptors [1]. The chemokine receptor family, which belongs to a superfamily of seven transmembrane domain G-protein-coupled receptors, comprises 18 members [2]. In 1996, one member, CXCR4, was identified as a coreceptor for the entry of T-cell line-tropic HIV-1 [3]. Since then, this receptor has attracted considerable attention as a pathogenic factor or a therapeutic target for HIV infection. Recent studies indicated that CXCR4 and its ligand, stromal cell-derived factor-1 (SDF-1), play an important role also in tumor metastasis [4–8]. Müller et al. [4] reported that CXCR4 was highly expressed in breast cancer and SDF-1 was highly expressed in organs representing the first destinations of metastasis. Moreover, they demonstrated that neutralization with anti-CXCR4 monoclonal antibody significantly inhibited the metastasis of breast cancer cells in mice. Similar results were obtained in other types of cancer [5–8]. These findings suggest that CXCR4 is a potential target for the in vivo imaging of metastatic tumors.

We have previously demonstrated that a peptide with anti-HIV-1 activity, T22 ([Tyr^{5,12}, Lys^{7}]-polyphemusin II), is an inhibitor of CXCR4 that blocks the entry of T-cell line-tropic HIV-1 mediated by this receptor. T22 is an 18-residue peptide amide, which was previously found by us based on an analysis of the structure–activity relationships of self-defense peptides of horseshoe crabs, tachyplesin and polyphemusin [9,10]. On the basis of the structure of T22, we designed and synthesized several downsized analogs, 14-residue peptides [11,12]. Among them, T140 showed the greatest inhibitory effect on the binding of an anti-CXCR4 monoclonal antibody to CXCR4 and the strongest inhibitory

* Corresponding author. Tel.: +81 75 753 4556; fax: +81 75 753 4568.
E-mail address: hsaji@pharm.kyoto-u.ac.jp (H. Saji).

0969-8051/$ – see front matter © 2006 Elsevier Inc. All rights reserved.
doi:10.1016/j.nucmedbio.2006.01.006

activity against HIV-1 entry [12]. The aim of this study was to develop a radiolabeled T140 derivative as an imaging agent for metastatic tumors. Considering that the three residues on the restricted backbone (L-3-(2-naphthyl)alanine (Nal)^3, Tyr^5 and Arg^{14}) and the single residue in the flexible region (Arg^2) form the intrinsic pharmacophore of T140 [13–15], we designed a 14-residue peptidic inhibitor, Ac-TZ14011, as the precursor for radiolabeled peptides (Fig. 1). This precursor contains the above four residues which are necessary for the inhibitory activity against CXCR4. Furthermore, for site-selective conjugation of radiolabels, Ac-TZ14011 has a single amino group (D-Lys^8), which is distant from the pharmacophore, and the carboxyl group of Arg^{14} of Ac-TZ14011 is protected via amidation for stability in vivo [16,17].

^{111}In constitutes one of the most useful radionuclides for the radiolabeling of peptides for diagnostic applications in nuclear medicine. Diethylenetriaminepentaacetic acid (DTPA) is still an attractive chelating agent with which to prepare ^{111}In-labeled peptides since it provides ^{111}In-labeled peptides with highly specific activity. In addition, the development of a monoreactive DTPA derivative has provided an easy and efficient way to prepare DTPA-conjugated peptides [18,19]. In this study, DTPA-Ac-TZ14011 was prepared using a monoreactive DTPA derivative and coordinated with nonradioactive In or radioactive ^{111}In. Furthermore, the antagonistic activity of In-DTPA-Ac-TZ14011 and in vivo behavior of ^{111}In-DTPA-Ac-TZ14011 were investigated and the applicability of ^{111}In-DTPA-Ac-TZ14011 as a radiopharmaceutical for imaging tumors was evaluated.

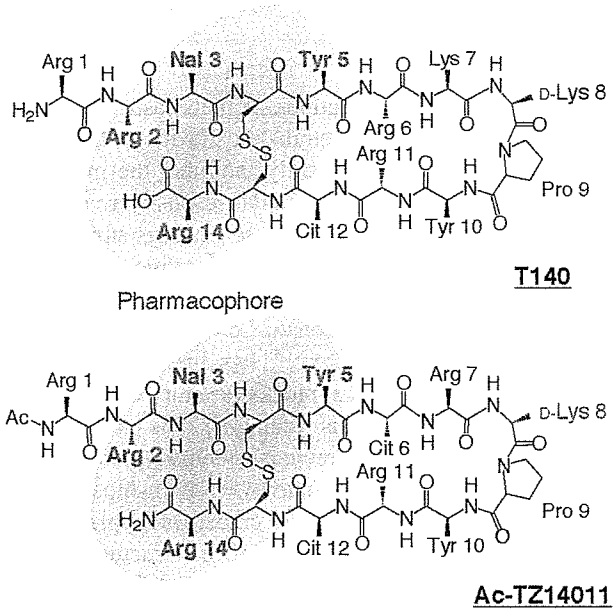

Fig. 1. Structures of T140 and Ac-TZ14011. There are four amino acid residues indispensable for the antagonistic activity (blue residues) which formed the pharmacophore. Nal: L-3-(2-naphthyl)alanine, Cit: L-citrulline. Ac-TZ14011 has a single amino group (D-Lys^8) for site-selective conjugation of radiolabels, which is distant from the pharmacophore.

2. Materials and methods

2.1. Reagents and chemicals

$^{111}InCl_3$ (74 MBq/ml in 0.02N HCl) was kindly supplied by Nihon Medi-Physics (Nishinomiya, Japan). 9-Fluorenylmethoxycarbonyl (Fmoc)-protected amino acids and 4-(2′,4′-dimethoxyphenylaminomethyl)phenoxy (SAL) resin were purchased from Watanabe Chemical Industries (Hiroshima, Japan) or Calbiochem-Novabiochem Japan (Tokyo, Japan). 1-*tert*-Butyl hydrogen 3,6,9-tris((*tert*-butoxycarbonyl)methyl)-3,6,9-triazaundecanedioic acid (mDTPA) was synthesized as reported previously [18]. All the other chemicals were purchased from either Nacalai Tesque (Kyoto, Japan) or Wako Pure Chemical Industries (Osaka, Japan). Ion spray mass spectra (IS-MS) were obtained with the API III model (PerkinElmer Sciex Instruments, Thornhill, Canada). Cellulose acetate electrophoresis (CAE) strips were run in veronal buffer (pH 8.6, I=0.06) at a constant current of 0.8 mA for 40 min. Thin-layer chromatography (TLC) analyses were performed with silica plates (Silica gel 60, Merck, Darmstadt, Germany) with 10% aqueous ammonium chloride–methanol (1:1) as the developing solvent.

2.2. Synthesis of In-DTPA-Ac-TZ14011

Fig. 2 shows the scheme for the synthesis of In-DTPA-Ac-TZ14011. A protected peptide was constructed using Fmoc-based solid-phase synthesis on SAL resin and its N-terminus was acetylated. After being treated with thioanisole/trifluoroacetic acid (TFA) in the presence of *m*-cresol and 1,2-ethanedithiol, the crude peptide was air-oxidized and purified by reversed-phase HPLC (RP-HPLC). RP-HPLC was carried out with a Cosmosil 5C18-AR column (20×250 mm, Nacarai Tesque) eluted with a linear gradient of 10–30% acetonitrile in 0.1% aqueous TFA in 30 min at a flow rate of 7 ml/min. Fractions containing the peptide were collected, and the solvent was removed by lyophilization to afford Ac-TZ14011 as a white powder. IS-MS calcd for $C_{92}H_{144}N_{35}O_{19}S_2$ [M+H$^+$]: *m/z* 2107.1, found: *m/z* 2107.4.

DTPA-Ac-TZ14011 was prepared by mDTPA conjugation. Briefly, to a solution of mDTPA (19 mg, 30.8 μmol) in acetonitrile (350 μl) were added *N*-hydroxysuccinimide (3.74 mg, 32.3 μmol) and *N*,*N*-dicyclohexylcarbodiimide (6.67 mg, 32.3 μmol) at 0°C, and the mixture was incubated overnight at room temperature. After cooling to 0°C again, 200 μl of Ac-TZ14011 (10.2 mg, 3.65 μmol) in a mixture of acetonitrile and phosphate-buffered saline (pH 7.4) (1:1) was added to the reaction mixture and incubated overnight at room temperature. After treatment with 95% TFA, the crude peptide was purified by RP-HPLC under the same conditions as above. IS-MS calcd for $C_{106}H_{165}N_{38}O_{28}S_2$ [M+H$^+$]: *m/z* 2482.2, found: *m/z* 2482.9.

Fifty microliters of DTPA-Ac-TZ14011 (610 μg, 0.20 μmol) in 0.1 M acetic acid was reacted with 25 μl of nonradioactive $InCl_3 \cdot 4H_2O$ (64.5 μg, 0.22 μmol) in 0.02N HCl for 30 min at room temperature. Subsequent

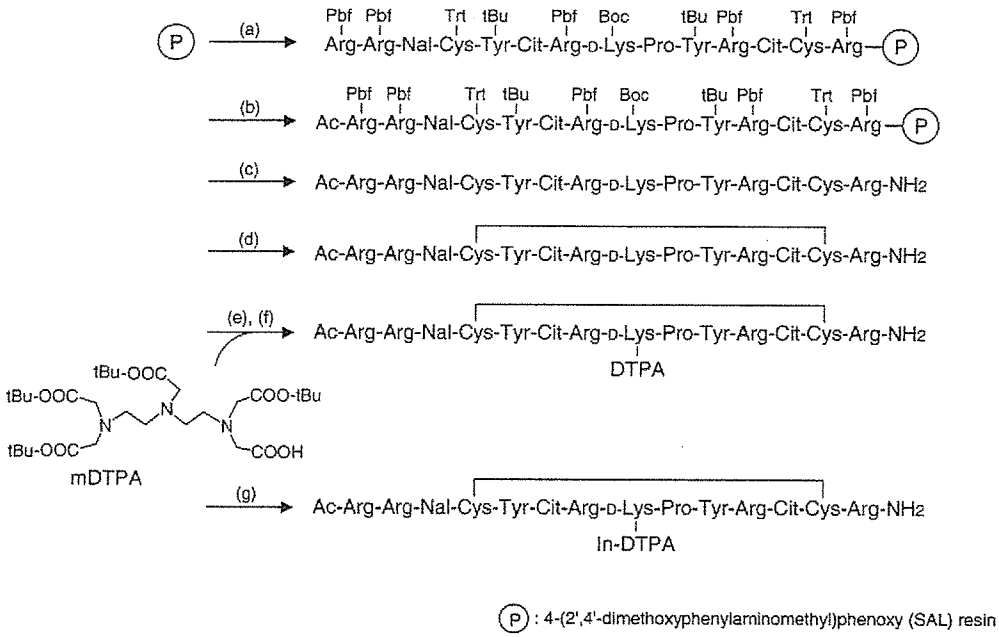

Fig. 2. Synthesis of In-DTPA-Ac-TZ14011. Reagents: (a) stepwise elongation; (b) acetic anhydride, pyridine; (c) trifluoroacetic acid, thioanisole, *m*-cresol, 1,2-ethanedithiol; (d) air oxidation; (e) *N*-hydroxysuccinimide, *N,N*-dicyclohexylcarbodiimide; (f) trifluoroacetic acid; (g) $InCl_3 \cdot 4H_2O$.

purification by RP-HPLC was carried out with a Hydrosphere C18 column (4.6×250 mm, YMC, Kyoto, Japan) eluted with 17% acetonitrile in 0.1% aqueous TFA at a flow rate of 1 ml/min. Fractions containing the peptide were collected, and the solvent was removed by lyophilization to afford In-DTPA-Ac-TZ14011 as a white powder. IS-MS calcd for $InC_{106}H_{161}N_{38}O_{28}S_2$ [$M+H^+$]: *m/z* 2594.2, found: *m/z* 2594.3.

2.3. Synthesis of ^{111}In-DTPA-Ac-TZ14011

$^{111}InCl_3$ (3.7 MBq) in 0.02N HCl (100 μl) was added to DTPA-Ac-TZ14011 (10 μg) in 0.1 M acetic acid (200 μl), and the mixture was incubated for 30 min at room temperature. Then, ^{111}In-DTPA-Ac-TZ14011 was separated from DTPA-Ac-TZ14011 by RP-HPLC under the same conditions used for the purification of In-DTPA-Ac-TZ14011. The radiochemical purity of ^{111}In-DTPA-Ac-TZ14011 was determined by TLC, CAE and RP-HPLC.

2.4. Binding assay

The binding assay was performed according to the procedure of Hesselgesser et al. [20] with a slight modification. The stable CXCR4-transfected Chinese hamster ovary (CHO) cell lines were prepared by transfection with cDNA encoding alanine scanning mutants in pcDNA3 (Invitrogen, Carlsbad, CA, USA) using lipofectamine (GIBCO, Rockville, MD, USA) and selection in neomycin (G418 500 mg/ml; GIBCO). The expression of CXCR4 on the surface of each transfectant was measured by flow cytometry. CXCR4-transfected CHO cell lines were suspended in the binding buffer (Ham's F-12 containing 20 mM HEPES and 0.5% BSA) and placed in siliconized tubes (5×10^5 cells/120 μl/tube). Binding reactions were performed on ice for 1 h in the presence of [^{125}I]SDF-1α (PerkinElmer Life Sciences, Boston, MA, USA) and various concentrations of peptides. Cells were separated from the buffer by centrifugation through a dibutylphthalate/olive oil mixture. After removal of the water and oil layer, cell-associated radioactivity was measured. The 50% inhibitory concentration (IC_{50}) of peptides was determined based on inhibition of the binding of SDF-1α to CXCR4-transfected CHO cells.

2.5. Calcium fluorimetry

Calcium fluorimetry was performed as described previously [21]. CXCR4-transfected CHO cell lines were placed in wells of a microtiter tray (3×10^4 cells/100 μl/well) and incubated for 1 day at 37°C in a CO_2 incubator. The cells were loaded with 5 μM of Fura-2-AM (Dojindo Laboratories, Kumamoto, Japan), 2.5 mM probenecid (Sigma, St Louis, MO, USA) and 20 mM HEPES (pH 7.4) in Ham's F-12 (80 μl/well) for 1 h at 37°C. After the cells were incubated with various concentrations of T140 analogs for 3 min, recombinant human SDF-1α (PeproTech EC, London, UK) was added. Changes in intracellular Ca^{2+} concentrations were measured by a spectrofluorometer (96-well Fluorescence Drug Screening System, Hamamatsu Photonix, Hamamatsu, Japan) using a modified version of the Fura-2 method [22]. The IC_{50} of peptides was determined based on the inhibition of Ca^{2+} mobilization induced by SDF-1α through CXCR4.

2.6. Biodistribution study in tumor-bearing mice

Animal experiments were conducted in accordance with our institutional guidelines and were approved by the Kyoto University Animal Care Committee. Athymic nude BALB/c

mice (8 weeks old, female) were inoculated subcutaneously with CXCR4-expressing pancreatic carcinoma cells, AsPC-1 [23,24]. When tumors were approximately 0.5 cm in diameter, the animals were intravenously injected with ^{111}In-DTPA-Ac-TZ14011 (25–30 kBq). The biodistribution of radioactivity was monitored at 1, 6 and 24 h postinjection. Groups of five mice were used for the experiments. Organs of interest were excised and weighed, and the radioactivity counts were determined with a well counter (ARC380CL, Aloka, Tokyo, Japan). For the in vivo blocking experiment, mice were coinjected with Ac-TZ14011 (10 mg/kg).

2.7. Statistical analysis

Statistical analysis was performed by using the unpaired *t*-test. $P<.05$ was considered to be statistically significant.

3. Results and discussion

T140 and its analogs have one disulfide bond and maintain an antiparallel β-sheet structure connected by a type II′ β-turn with D-Lys^8-Pro^9 at the (*i*+1) and (*i*+2) positions, and the side chain of D-Lys^8 is distant from the pharmacophore for the antagonistic activity [14,15]. Therefore, we designed Ac-TZ14011 as a mother compound that contains the residues indispensable for the antagonistic activity and has a single amino group of D-Lys^8 for site-selective conjugation of DTPA (Fig. 1). In calcium fluorimetric assays, this compound showed strong inhibitory activity equal to that of T140 (Table 1). To assess the effect of the conjugation of In-DTPA with Ac-TZ14011 on the antagonistic activity toward CXCR4, nonradioactive In-DTPA-Ac-TZ14011 was synthesized (Fig. 2). In binding assays with CXCR4, In-DTPA-Ac-TZ14011 maintained strong inhibitory activity although its IC_{50} value was slightly larger than that of Ac-TZ14011 (Table 1). This result indicated the validity of the chemical design of In-DTPA-Ac-TZ14011 based on structure–activity relationships.

In RP-HPLC analyses, In-DTPA-Ac-TZ14011 and DTPA-Ac-TZ14011 showed well-separated peaks as shown in Fig. 3. After purification by RP-HPLC under the same conditions, ^{111}In-DTPA-Ac-TZ14011 was obtained with high radiochemical purity (over 96%) as determined by TLC, CAE and RP-HPLC. The radioactivity pharmacokinetics of ^{111}In-DTPA-Ac-TZ14011 was evaluated in nude mice bearing the CXCR4-expressing pancreatic carcinoma AsPC-1 (Table 2). ^{111}In-DTPA-Ac-TZ14011 showed a rapid clearance from the blood and a marked accumulation and retention in the liver, kidney and spleen. The accumulation of radioactivity was greater in the tumor than in the blood or muscle (Table 2). In mice, CXCR4 mRNA is highly expressed in various lymphoid tissues and cells such as spleen, thymus, lymph node, bone marrow and leukocytes [25,26]. Thus, since liver and spleen are concerned with the immune system, the accumulation of ^{111}In-DTPA-Ac-TZ14011 in these organs should be mediated by CXCR4-binding. In fact, coinjection of Ac-TZ14011 significantly reduced the accumulation in the liver by over one-tenth and in the spleen by over one-third. This marked reduction of radioactivity in the liver and spleen on the coinjection of Ac-TZ14011 caused the high levels of radioactivity in the blood and consequently increased the accumulation of radioactivity in organs which were small in size and/or did not take up much radioactivity (Table 2). The accumulation in the tumor was also increased by coinjection of Ac-TZ14011, but the tumor-to-blood and tumor-to-muscle ratios were significantly reduced (Table 2). Since there is very little or no CXCR4 in the muscle [26],

Table 1
Antagonistic activity of T140 derivatives

	IC_{50} (nM)	
	SDF-1α binding[a]	Ca^{2+} mobilization[b]
In-DTPA-Ac-TZ14011	7.9	ND[c]
Ac-TZ14011	1.2	2.6
T140	ND[c]	2.2

[a] Values are the concentrations for 50% inhibition of the binding of [^{125}I]SDF-1α to CXCR4.

[b] Values are the concentrations for 50% inhibition of Ca^{2+} mobilization induced by SDF-1á through CXCR4.

[c] Not determined.

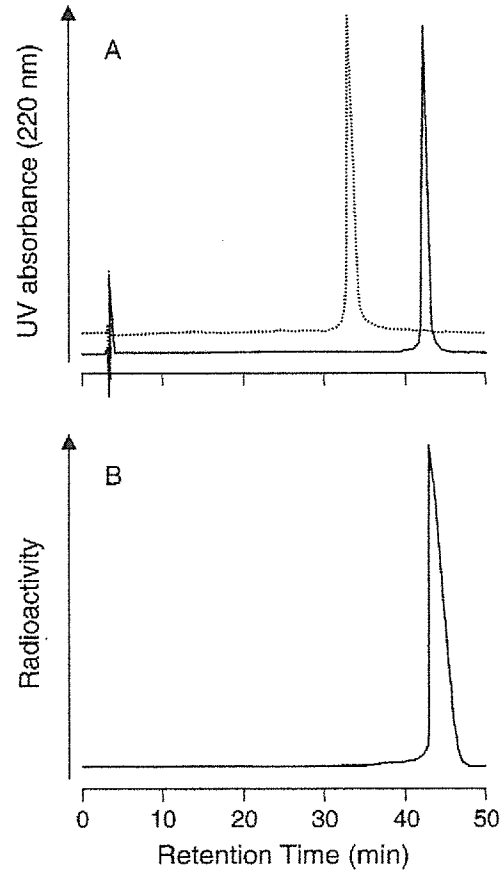

Fig. 3. Reversed-phase HPLC profiles of nonradioactive In-DTPA-Ac-TZ14011 (solid line), DTPA-Ac-TZ14011 (broken line) (A) and ^{111}In-DTPA-Ac-TZ14011 (B).

Table 2
Biodistribution of radioactivity after intravenous injection of ^{111}In-DTPA-Ac-TZ14011 in nude mice bearing pancreatic carcinoma, AsPC-1

	1 h	6 h	24 h	1 h+ Ac-TZ14011[a]
Blood[b]	0.39 (0.06)	0.05 (0.01)	0.03 (0.01)	2.06** (0.61)
Liver[b]	27.0 (2.9)	25.2 (2.0)	19.3 (2.5)	1.95** (0.25)
Kidney[b]	50.9 (4.3)	43.4 (6.3)	29.5 (5.7)	45.4 (6.8)
Spleen[b]	8.22 (0.70)	7.57 (0.54)	5.83 (0.99)	2.66** (1.21)
Pancreas[b]	0.15 (0.03)	0.05 (0.01)	0.05 (0.02)	1.07** (0.46)
Muscle[b]	0.17 (0.05)	0.07 (0.02)	0.07 (0.01)	1.35** (0.26)
Tumor[b]	0.51 (0.08)	0.20 (0.03)	0.14 (0.03)	1.70** (0.27)
T/B ratio[c]	1.31 (0.14)	4.05 (0.79)	5.65 (2.89)	0.88* (0.31)
T/M ratio[d]	3.17 (0.99)	4.43 (1.89)	3.23 (1.08)	1.31** (0.41)

Each value represents the mean (S.D.) for five animals.
[a] Coinjection with unlabeled Ac-TZ14011 (10 mg/kg).
[b] Expressed as % injected dose per gram.
[c] Tumor-to-blood ratio.
[d] Tumor-to-muscle ratio.
* $P<.05$, comparison between ^{111}In-DTPA-Ac-TZ14011 with or without unlabeled Ac-TZ14011 at 1 h.
** $P<.005$, comparison between ^{111}In-DTPA-Ac-TZ14011 with or without unlabeled Ac-TZ14011 at 1 h.

tumor-to-muscle ratios reflect target-to-nontarget ratios. Thus, the reduction in the tumor-to-muscle ratio caused by the coinjection of Ac-TZ14011 indicated that ^{111}In-DTPA-Ac-TZ14011 accumulated in the tumor through CXCR4. On the other hand, coinjection of Ac-TZ14011 did not alter the levels of ^{111}In-DTPA-Ac-TZ14011 in the kidney, suggesting a nonspecific accumulation. This is consistent with previous findings that CXCR4 mRNA levels expressed in the kidney were very low [25,26]. Recent studies indicated that an electrostatic interaction between positively charged peptides and the negatively charged surface of renal proximal tubular cells plays an important role in the reabsorption of peptides into proximal tubular cells [27–29]. Since five Arg residues are contained in the peptide ^{111}In-DTPA-Ac-TZ14011, the highly positive charge would cause a greater nonspecific accumulation in the kidney even compared to other ^{111}In-DTPA peptides [28,30,31]. Due to its accumulation in nontarget organs, ^{111}In-DTPA-Ac-TZ14011 may be unavailable as a radiopharmaceutical for screening small tumors, particularly in the kidneys and their surroundings.

It was reported that CXCR4 expression could be a powerful predictive factor for prognosis (recurrence, metastasis or survival rate) in colorectal cancer [32,33], malignant melanoma [34] and osteosarcoma [35]. Therefore, a CXCR4 imaging agent would be a new type of radiopharmaceutical for predicting the prognosis of cancer patients. CXCR4 also represents a novel target for tumor therapy, and some CXCR4 inhibitors have been investigated as anti-metastatic agents [36–39]. These agents showed positive effects in suppressing tumor metastasis; however, they would also have deleterious effects on normal physiological functions since CXCR4 plays a crucial role in numerous biological processes [2]. Therefore, in vivo imaging of CXCR4 expression could be a potential method for determining the dose of anti-metastatic agents and for monitoring their therapeutic efficacy.

In conclusion, we designed ^{111}In-DTPA-Ac-TZ14011 based on the structure–activity relationships of peptidic CXCR4 inhibitors. In-DTPA-Ac-TZ14011 showed strong inhibitory activity against the binding of CXCR4 to an endogenous ligand. Furthermore, the accumulation of ^{111}In-DTPA-Ac-TZ14011 in the CXCR4-expressing tumor was greater than that in the blood or muscle, being mediated by this receptor. These findings suggest that ^{111}In-DTPA-Ac-TZ14011 is a potential radiopharmaceutical for the imaging of CXCR4 expression in metastatic tumors in vivo for predicting the prognosis of cancer patients and for monitoring the therapeutic efficacy of anti-metastatic agents.

Acknowledgments

We are grateful to Nihon Medi-Physics (Nishinomiya, Japan) for the gift of $^{111}InCl_3$. This work was supported in part by a Grant-in-Aid for Cancer Research from the Ministry of Health, Labour and Welfare.

References

[1] Zlotnik A, Yoshie O. Chemokines: a new classification system and their role in immunity. Immunity 2000;12:121–7.
[2] Horuk R. Chemokine receptors. Cytokine Growth Factor Rev 2001;12:313–35.
[3] Feng Y, Broder CC, Kennedy PE, Berger EA. HIV-1 entry cofactor: functional cDNA cloning of a seven-transmembrane, G protein-coupled receptor. Science 1996;272:872–7.
[4] Müller A, Homey B, Soto H, Ge N, Catron D, Buchanan ME, et al. Involvement of chemokine receptors in breast cancer metastasis. Nature 2001;410:50–6.
[5] Taichman RS, Cooper C, Keller ET, Pienta KJ, Taichman NS, McCauley RS. Use of the stromal cell-derived factor-1/CXCR4 pathway in prostate cancer metastasis to bone. Cances Res 2002;62:1832–7.
[6] Schrader AJ, Lechner O, Templin M, Dittmar KEJ, Machtens S, Mengel M, et al. CXCR4/CXCL12 expression and signaling in kidney cancer. Br J Cancer 2002;86:1250–6.
[7] Phillips RJ, Burdick MD, Lutz M, Belperio JA, Keane MP, Strieter RM. The stromal derived factor-1/CXCL12-CXC chemokine receptor 4 biological axis in non-small cell lung cancer metastases. Am J Respir Crit Care Med 2003;167:1676–86.
[8] Uchida D, Begum NM, Almofti A, Nakashiro K, Kawamata H, Tateishi Y, et al. Possible role of stromal-cell-derived factor-1/CXCR4 signaling on lymph node metastasis of oral squamous cell carcinoma. Exp Cell Res 2003;290:289–302.
[9] Masuda M, Nakashima H, Ueda T, Naba H, Ikoma R, Otaka A, et al. A novel anti-HIV synthetic peptide, T-22 ([Tyr^{5,12}Lys^{7}]-polyphemusin II). Biochem Biophys Res Commun 1992;189:845–50.
[10] Murakami T, Nakajima T, Koyanagi Y, Tachibana K, Fujii N, Tamamura H, et al. A small molecule CXCR4 inhibitor that blocks T cell line-tropic HIV-1 infection. J Exp Med 1997;186:1389–93.
[11] Tamamura H, Arakaki R, Funakoshi H, Imai M, Otaka A, Ibuka T, et al. Effective lowly cytotoxic analogs of an HIV-cell fusion inhibitor, T22 ([Tyr^{5,12},Lys^{7}]-polyphemusin II). Bioorg Med Chem 1998;6:231–8.
[12] Tamamura H, Xu Y, Hattori T, Zhang X, Arakaki R, Kanbara K, et al. A low-molecular- weight inhibitor against the chemokine receptor

CXCR4: a strong anti-HIV peptide T140. Biochem Biophys Res Commun 1998;253:877–82.

[13] Tamamura H, Omagari A, Oishi S, Kanamoto T, Yamamoto N, Peiper SC, et al. Pharmacophore identification of a specific CXCR4 inhibitor, T140, leads to development of effective anti-HIV agents with very high selectivity indexes. Bioorg Med Chem Lett 2000;10:2633–7.

[14] Tamamura H, Sugioka M, Odagaki Y, Omagari A, Kan Y, Oishi S, et al. Conformational study of a highly specific CXCR4 inhibitor, T140, disclosing the close proximity of its intrinsic pharmacophores associated with strong anti-HIV activity. Bioorg Med Chem Lett 2001;11:359–62.

[15] Tamamura H, Sugioka M, Odagaki Y, Omagari A, Kan Y, Oishi S, et al. Corrigendum to "conformational study of a highly specific CXCR4 inhibitor, T140, disclosing the close proximity of its intrinsic pharmacophores associated with strong anti-HIV activity" [Bioorg. Med. Chem. Lett. 11 (2001) 359]. Bioorg Med Chem Lett 2001;11:2409.

[16] Tamamura H, Omagari A, Hiramatsu K, Gotoh K, Kanamoto T, Xu Y, et al. Development of specific CXCR4 inhibitors possessing high selectivity indexes as well as complete stability in serum based on an anti-HIV peptide T140. Bioorg Med Chem Lett 2001;11:1897–902.

[17] Tamamura H, Hiramatsu K, Kusano S, Terakubo S, Yamamoto N, Trent JO, et al. Synthesis of potent CXCR4 inhibitors possessing low cytotoxicity and improved biostability based on T140 derivatives. Org Biomol Chem 2003;1:3656–62.

[18] Arano Y, Uezono T, Akizawa H, Ono M, Wakisaka K, Nakayama M, et al. Reassessment of diethylenetriaminepentaacetic acid (DTPA) as a chelating agent for indium-111 labeling of polypeptides using a newly synthesized monoreactive DTPA derivative. J Med Chem 1996;39: 3451–60.

[19] Arano Y, Akizawa H, Uezono T, Akaji K, Ono M, Funakoshi S, et al. Conventional and high-yield synthesis of DTPA-conjugated peptide: application of a monoreactive DTPA to DTPA-D-Phe^1-octreotide synthesis. Bioconjug Chem 1997;8:442–6.

[20] Hesselgesser J, Liang M, Hoxie J, Greenberg M, Brass LF, Orsini MJ, et al. Identification and characterization of CXCR4 chemokine receptor in human T cell lines: ligand binding, biological activity, and HIV-1 infectivity. J Immunol 1998;160:877–83.

[21] Tamamura H, Omagari A, Hiramatsu K, Oishi S, Habashita H, Kanamoto T, et al. Certification of the critical importance of L-3-(2-naphthyl)alanine at position 3 of specific CXCR4 inhibitor, T140, leads to an exploratory performance of its downsizing study. Bioorg Med Chem 2002;10:1417–26.

[22] Grynkiewicz G, Poenie M, Tsien RY. A new generation of Ca^{2+} indicators with greatly improved fluorescence properties. J Biol Chem 1985;260:3440–50.

[23] Koshiba T, Hosotani R, Miyamoto Y, Ida J, Tsuji S, Nakajima S, et al. Expression of stromal cell-derived factor 1 and CXCR4 ligand receptor system in pancreatic cancer: a possible role for tumor progression. Clin Cancer Res 2000;6:3530–5.

[24] Mori T, Doi R, Koizumi M, Toyoda E, Ito D, Kami K, et al. CXCR4 antagonist inhibits stromal cell-derived factor 1-induced migration and invasion of human pancreatic cancer. Mol Cancer Ther 2004;3: 29–37.

[25] Nagasawa T, Nakajima T, Tachibana K, Iizasa H, Bleul CC, Yoshie O, et al. Molecular cloning and characterization of a murine pre-B-cell growth-stimulating factor/stromal cell-derived factor 1 receptor, a murine homolog of the human immunodeficiency virus 1 entry coreceptor fusin. Proc Natl Acad Sci U S A 1996;93:14726–9.

[26] Moepps B, Frodl R, Rodewald HR, Bsggiolini M, Gierschik P. Two murine homologues of the human chemokine receptor CXCR4 mediating stromal cell-derived factor 1α activation of G_{i2} are differentially expressed in vivo. Eur J Immunol 1997;27: 2102–12.

[27] de Jong M, Rolleman EJ, Bernard BF, Visser TJ, Bakker WH, Breeman WAP, et al. Inhibition of renal uptake of indium-111-DTPA-octreotide in vivo. J Nucl Med 1996;37:1388–92.

[28] Akizawa H, Arano Y, Mifune M, Iwado A, Saito Y, Mukai T, et al. Effect of molecular charges on renal uptake of ^{111}In-DTPA-conjugated peptides. Nucl Med Biol 2001;28:761–8.

[29] Akizawa H, Takimoto H, Saito M, Iwado A, Mifune M, Saito Y, et al. Effect of carboxylation of N-terminal phenylalanine of ^{111}In-DTPA (diethylenetriaminepentaacetic acid)-octreotide on accumulation of radioactivity in kidney. Biol Pharm Bull 2004;27:271–2.

[30] Bagutti C, Stolz B, Albert R, Bruns C, Pless J, Eberle AN. [^{111}In]-DTPA-labeled analogues of α-melanocyte-stimulating hormone for melanoma targeting: receptor binding in vitro and in vivo. Int J Cancer 1994;58:749–55.

[31] de Visser M, Janssen PJJM, Srinvasan A, Reubi JC, Waser B, Erion JL, et al. Stabilised ^{111}In-labelled DTPA- and DOTA-conjugated neurotensin analogues for imaging and therapy of exocrine pancreatic cancer. Eur J Nucl Med Mol Imaging 2003;30:1134–9.

[32] Schimanski CC, Schwald S, Simiantonaki N, Jayasinghe C, Gonner V, Wilsberg V, et al. Effect of chemokine receptors CXCR4 and CCR7 on the metastatic behavior of human colorectal cancer. Clin Cancer Res 2005;11:1743–50.

[33] Kim J, Takeuchi H, Lam ST, Turner RR, Wang HJ, Kuo C, et al. Chemokine receptor CXCR4 expression in colorectal cancer patients increases the risk for recurrence and for poor survival. J Clin Oncol 2005;23:2744–53.

[34] Scala S, Ottaiano A, Ascierto PA, Cavalli M, Simeone E, Giuliano P, et al. Expression of CXCR4 predicts poor prognosis in patients with malignant melanoma. Clin Cancer Res 2005;11:1835–41.

[35] Laverdiere C, Hoang BH, Yang R, Sowers R, Qin J, Meyers PA, et al. Messenger RNA expression levels of CXCR4 correlate with metastatic behavior and outcome in patients with osteosarcoma. Clin Cancer Res 2005;11:2561–7.

[36] Tamamura H, Hori A, Kanzaki N, Hiramatsu K, Mizumoto M, Nakashima H, et al. T140 analogs as CXCR4 antagonists identified as anti-metastatic agents in the treatment of breast cancer. FEBS Lett 2003;550:79–83.

[37] Liang Z, Wu T, Lou H, Yu X, Taichman RS, Lau SK, et al. Inhibition of breast cancer metastasis by selective synthetic polypeptide against CXCR4. Cancer Res 2004;64:4302–8.

[38] Takenaga M, Tamamura H, Hiramatsu K, Nakamura N, Yamaguchi Y, Kitagawa A, et al. A single treatment with micro-capsules containing a CXCR4 antagonist suppresses pulmonary metastasis of murine melanoma. Biochem Biophys Res Commun 2004;320:226–32.

[39] Smith MC, Luker KE, Garbow JR, Prior JL, Jackson E, Piwnica-Worms D, et al. CXCR4 regulates growth of both primary and metastatic breast cancer. Cancer Res 2004;64:8604–12.

Brief Articles

Identification of a New Class of Low Molecular Weight Antagonists against the Chemokine Receptor CXCR4 Having the Dipicolylamine−Zinc(II) Complex Structure

Hirokazu Tamamura,*,† Akio Ojida,‡ Teppei Ogawa,§ Hiroshi Tsutsumi,† Hiroyuki Masuno,† Hideki Nakashima,∥ Naoki Yamamoto,⊥ Itaru Hamachi,‡ and Nobutaka Fujii*,§

Institute of Biomaterials and Bioengineering, Tokyo Medical and Dental University, Chiyoda-ku, Tokyo 101-0062, Japan, Graduate School of Engineering, Kyoto University, Nishikyo-ku, Kyoto 615-8510, Japan, Graduate School of Pharmaceutical Sciences, Kyoto University, Sakyo-ku, Kyoto 606-8501, Japan, School of Medicine, St. Marianna University, Miyamae-ku, Kawasaki 216-8511, Japan, and AIDS Research Center, National Institute of Infectious Diseases, Shinjuku-ku, Tokyo 162-8640, Japan

Received January 10, 2006

Several low molecular weight nonpeptide compounds having the dipicolylamine−zinc(II) complex structure were identified as potent and selective antagonists of the chemokine receptor CXCR4. These compounds showed strong inhibitory activity against CXCL12 binding to CXCR4, and the top compound exhibited significant anti-HIV activity. Zinc(II)−dipicolylamine unit-containing compounds proved to be useful and attractive lead compounds for chemotherapy of these diseases as nonpeptide CXCR4 antagonists possessing the novel scaffold structure.

Introduction

CXCR4 is a chemokine receptor that transduces signals of its endogenous ligand, CXCL12/stromal cell-derived factor-1 (SDF-1).[1−4] CXCR4 is classified into 7TMGPCR and plays a physiologically critical role by the action of CXCL12 in the migration of progenitors during embryologic development of the cardiovascular, hemopoietic, central nervous systems, etc. In addition, CXCR4 was previously identified as a coreceptor that is used by X4-HIV-1 in its entry into T cells[5] and has recently been proven to be involved in several problematic diseases, including HIV infection, metastasis of several types of cancer,[6−8] leukemia cell progression,[9,10] rheumatoid arthritis (RA).[11,12] Thus, CXCR4 is thought to be a great therapeutic target to overcome these diseases, and several inhibitors directed against CXCR4 have been developed to date.[13−22] We previously found a highly potent CXCR4 antagonist, T140, which is a 14-mer peptide with a disulfide bridge, and its downsized derivative, FC131, which has a cyclic pentapeptide scaffold structure (Table 1).[18−21] Although reduction of the peptide character based on these peptides is underway,[23,24] we would like to discover novel CXCR4 antagonists having nonpeptide structures, since few nonpeptide compounds with low molecular weight have been reported, such as AMD3100 series[14,16] and KRH-1636.[22] Previously, anthracene derivatives having two sets of zinc(II)−2,2′-dipicolylamine (Dpa) complex were identified as the first chemosensors that can selectively bind and sense phosphorylated peptide surfaces.[25] In the present study, we have found several aromatic compounds having the zinc(II)−Dpa structure to be a new class of low molecular weight CXCR4 antagonists.

* Corresponding authors. H.T.: tel, +81 3 5280 8036; fax, +81 3 5280 8039; e-mail, tamamura.mr@tmd.ac.jp. N.F.: tel, +81 75 753 4551; fax, +81 75 753 4570; e-mail, nfujii@pharm.kyoto-u.ac.jp.
† Tokyo Medical and Dental University.
‡ Graduate School of Engineering, Kyoto University.
§ Graduate School of Pharmaceutical Sciences, Kyoto University.
∥ St. Marianna University.
⊥ National Institute of Infectious Diseases.

Experimental Section

Chemistry. Synthesis of Bis(dipicolylamine)-*p*-xylene−Zn Complexes. Aromatic compounds having the zinc(II)−Dpa structure were previously synthesized as reported elsewhere.[25−28]

For a comparative study, bis(3,3′- and bis(4,4′-dipicolylamine)-*p*-xylenes, **24** and **25**, respectively, were synthesized by treatment of *p*-xylenediamine with the corresponding pyridinecarbaldehydes and sodium triacetoxyborohydride [$NaBH(OAc)_3$] (Figure 1).[29] Zinc(II) complexation in the preparation of **18** and **19** was performed by treatment of bis(dipicolylamine)-*p*-xylenes with NaOH to afford salt-free compounds, followed by addition of aqueous zinc nitrate [$Zn(NO_3)_2$].

Biological Assays. Calcium mobilization,[30] [^{125}I]CXCL12 binding (oil cushion method),[30] and anti-HIV[23] assays were performed as reported previously.

Molecular Modeling Calculations. Molecular modeling calculations were performed using SYBYL program (version 7.0, TRIPOS Inc.). Energy minimizations were performed using Tripos force field. The lowest energy conformation was obtained by random search method.

Biological Results and Discussion

Several aromatic compounds having the zinc(II)−dipicolylamine structure were prepared and surveyed for CXCR4-antagonistic activity based on inhibitory activity against Ca^{2+} mobilization induced by CXCL12 stimulation through CXCR4. The structures and CXCR4-antagonistic activity of these compounds are shown in Tables 1−3. Positive controls **8** (T140), **9** (FC131), and **10** (KRH-1636) showed strong antagonistic activity. Compound **2**, which has two sets of the [bis(pyridin-2-ylmethyl)amino]methylene unit with zinc(II) complexation at the para-position of benzene, showed potent CXCR4-antagonistic activity ($IC_{50} = 0.1\ \mu M$). Compound **1**, which has a piece of this unit, did not show any activity until 1 μM. It suggests that two sets of this unit are required for binding to CXCR4. Compound **3**, which has two sets of this unit at the meta-position of benzene, showed lower activity than compound **2**, suggesting that the presence of this unit at the para-position is critical for

10.1021/jm060025u CCC: $33.50
Published on Web 05/03/2006

Table 1. Structures and CXCR4-Antagonistic Activity of Aromatic Compounds Having the Zinc(II)−Dipicolylamine Structure (I)

Compd. (No.)	Structure	IC_{50} (μM)[a]
1	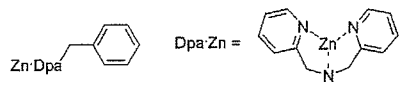	> 1
2	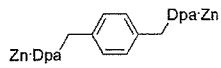	0.10
3	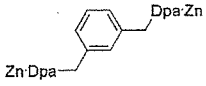	0.49
4	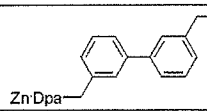	0.35
5	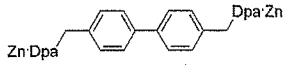	0.12
6	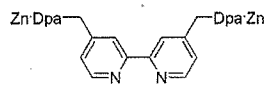	0.46
7	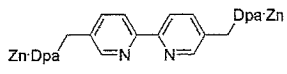	0.10
8	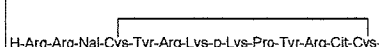 T140	0.0036
9	*cyclo*(-Nal-Gly-D-Tyr-Arg-Arg-) FC131	0.036
10	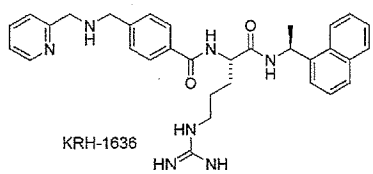	0.040

[a] IC_{50} values are based on the inhibition against Ca^{2+} mobilization induced by CXCL12 stimulation through CXCR4. All data are the mean values for at least two independent experiments.

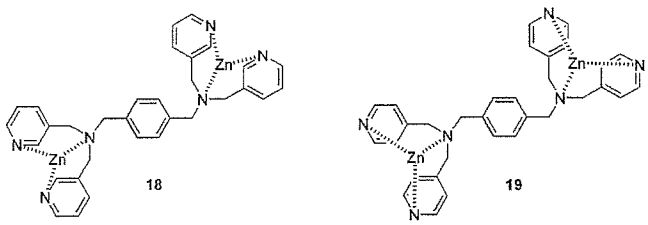

Figure 1. Structures of the zinc(II)−bis(3,3′- and −bis(4,4′-dipicolylamine)-*p*-xylene (**24** and **25**) complexes, **18** and **19**, respectively.

strong CXCR4-antagonistic activity. Biphenyl compounds having two sets of this unit at the 3,3′- and 4,4′-positions, **4** and **5**, respectively, exhibited significantly high antagonistic activity, although the compound with the 4,4′-positions substituted (**5**) is stronger than that having the 3,3′-positions substituted (**4**). It seems to be important that two sets of the [bis(pyridin-2-ylmethyl)amino]methylene unit with zinc(II) complexation are

Table 2. Structures and CXCR4-Antagonistic Activity of Aromatic Compounds Having the Zinc(II)−Dipicolylamine Structure (II)

Compd. (No.)	Structure	IC_{50} (μM)
11	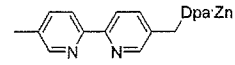	> 1
12	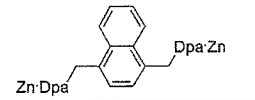	0.18
13	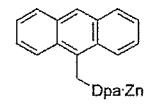	0.77
14	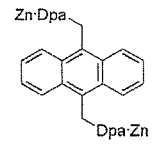	0.24
15	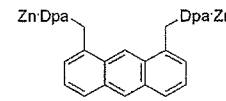	0.75
16	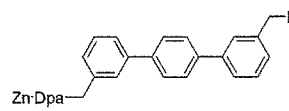	> 1
17	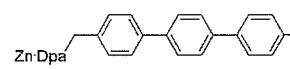	> 1

Table 3. Structures and CXCR4-Antagonistic Activity of Aromatic Compounds Having the Zinc(II)−Dipicolylamine Structure and Zinc-Free Compounds

compd	structure	IC_{50} (μM)
18	shown in Figure 1	>10
19	shown in Figure 1	>10
20	zinc-free analogue of **2**	>10
21	zinc-free analogue of **5**	>10
22	zinc-free analogue of **7**	>10
23	zinc-free analogue of **14**	>10
24	zinc-free analogue of **18**	>10
25	zinc-free analogue of **19**	>10

located at 180° of each other as in compounds **2** and **5**, which both have almost the same potency. Furthermore, replacement of the biphenyl unit of compounds **4** and **5** by [2,2′]bipyridinyl did not cause significant change in CXCR4-antagonistic activity, since the [2,2′]bipyridinyl compounds **6** and **7** showed almost the same potency as the biphenyl compounds **4** and **5**, respectively. It may be a matter of course that a [2,2′]bipyridinyl compound having only one [bis(pyridin-2-ylmethyl)amino]-methylene unit with zinc(II) complexation (**11**) did not show any activity until 1 μM, as compound **1** did not. A naphthyl compound (**12**) and an anthracenyl compound (**14**), which have two sets of this unit at the 1,4-positions and at the 9,10-positions,